Mid-Holocene Climate Change over China: Model-Data Discrepancy

Yating Lin [1,2,4], Gilles Ramstein [2], Haibin Wu [1,3,4], Raj Rani [2], Pascale Braconnot [2], Masa Kageyama [2], Qin Li [1,3], Yunli Luo [5], Ran Zhang [6] and Zhengtang Guo [1,3,4]

1. Key Laboratory of Cenozoic Geology and Environment, Institute of Geology and Geophysics, Chinese Academy of Sciences, Beijing 100029, China

2. Laboratoire des Sciences du Climat et de l'Environnement, LSCE/IPSL, CEA-CNRS-UVSQ, Université Paris-Saclay, Gif-sur-Yvette 91191, France

3. CAS Center for Excellence in Life and Paleoenvironment, Beijing, 100044, China

4. University of Chinese Academy of Sciences, Beijing 100049, China

5. Institute of Botany, Chinese Academy of Sciences, Beijing 100093, China

6. Institute of Atmospheric Physics, Chinese Academy of Sciences, Beijing 100029, China

Abstract:

The mid-Holocene period (MH) has long been an ideal target for the validation of Global Circulation Model (GCM) results against reconstructions gathered in global datasets. These studies aim to test the GCM sensitivity mainly to the seasonal changes induced by the orbital parameters (precession). Despite widespread agreement between model results and data on the MH climate, some important differences still exist. There is no consensus on the continental size (the area of the temperature anomaly) of the MH thermal climate response, which makes regional quantitative reconstruction critical to obtain a comprehensive understanding of the MH climate patterns. Here, we compare the annual and seasonal outputs from the most recent Paleoclimate Modelling Intercomparison Project Phase 3 (PMIP3) models with an updated synthesis of climate reconstruction over China, including, for the first time, a seasonal cycle of temperature and precipitation. Our results indicate that the main discrepancies between model and data for the MH climate are the annual and winter mean temperature. A warmer-than-present climate condition is derived from pollen data for both annual mean

temperature (~0.7 K on average) and winter mean temperature (~1 K on average), while most of the models provide both colder-than-present annual and winter mean temperature and a relatively warmer summer, showing linear response driven by the seasonal forcing. By conducting simulations in BIOME4 and CESM, we show that the surface processes are the key factors drawing the uncertainties between models and data. These results pinpoint the crucial importance of including the non-linear responses of the surface water and energy balance to vegetation changes.

Keywords: PMIP3 Pollen data Inverse Vegetation Model Seasonal climate change

1. Introduction

Much attention of paleoclimate study has been focused on the current interglacial (the Holocene), especially the mid-Holocene (MH, 6±0.5 ka). The major difference in the experimental configuration between the MH and pre-Industrial (PI) arises from the orbital parameters which brings about an increase in the amplitude of the seasonal cycle of insolation of the Northern Hemisphere and a decrease in the Southern Hemisphere (Berger, 1978). Thus, the MH provides an excellent case study on which to base an evaluation of the climate response to changes in the distribution of insolation. Great efforts are devoted by the modeling community to the design of the MH common experiments using similar boundary conditions (Joussaume and Taylor., 1995; Harrison et al., 2002; Braconnot et al., 2007a, b). In addition, much work has been done to reconstruct the paleoclimate change based on different proxies at global and continental scale (Guiot et al., 1993; Kohfeld and Harrison, 2000; Prentice et al.,

2000; Bartlein et al., 2011). The greatest progress in understanding the MH climate change and variability has consistently been made by comparing large-scale analyses of data with simulations from global climate models (Joussaume et al., 1999; Liu et al., 2004; Harrison et al., 2014).

However, the source of discrepancies between model and data is still an open and stimulating question. Two types of inconsistencies have been identified: 1) where the model and data show opposite signs, for instance, paleoclimate evidence from data-records indicates an increase of about 0.5 K in global annual mean temperature during the MH compared with PI (Shakun et al.. 2012; Marcott et al., 2013), while there is a cooling trend in model simulations (Liu et al., 2014). 2) where the same trend is displayed by both model and data but with different magnitudes. Previous studies have shown that while climate models can successfully reproduce the direction and large-scale patterns of past climate changes, they tend to consistently underestimate the magnitude of change in the monsoons of the Northern Hemisphere as well as the amount of the MH precipitation over northern Africa (Braconnot et al., 2012; Harrison et al., 2015). Moreover, significant spatial variability has been noted in both observations and simulations (Peyron et al., 2000; Davis et al., 2003; Braconnot et al., 2007a; Wu et al., 2007; Bartlein et al., 2011). For instance, Marcott et al. (2013) reconstructed a cooling trend of global temperature during Holocene, mainly from the marine records (~80%). While based on 642 sub-fossil pollen data, Marsicek et al. (2018) shows a long-term warming defined the Holocene until around 2000 years ago for Europe and North America continents. The different trends of pollen- and marine-based reconstruction indicate the spatial variability of annual temperature change during MH over the globe, which has already been investigated by Bartlein et al. (2010). That makes regional quantitative reconstruction (Davis et al., 2003; Mauri et al., 2015) essential to obtain a comprehensive understanding of the MH climate patterns, and to act as a benchmark to evaluate climate models (Fischer and Jungclaus, 2011; Harrison et al., 2014;).

China offers two advantages in respect to these issues. The sheer expanse of the country means that the continental response to insolation changes over a large region can be investigated. Moreover, the quantitative reconstruction of seasonal climate changes during the MH, based on the new pollen dataset, provides a unique opportunity to compare the seasonal cycles for models and data. Previous studies indicate that warmer and wetter than present conditions prevailed over China during the MH and that the magnitude of the annual temperature increases varied from 2.4-5.8 K spatially, with an annual precipitation increase in the range of 34-267 mm (e.g., Sun et al., 1996; Jiang et al., 2010; Lu et al., 2012; Chen et al., 2015). However, Jiang et al. (2012) clearly show a mismatch between multi-proxy reconstructions and model simulations. In terms of climate anomalies (MH-PI), besides the ~1 K increase in summer temperature, 35 out of 36 Paleoclimate Modelling Intercomparison Projects (PMIP) models reproduce annual (~0.4 K) and winter temperatures (~1.4 K) that are colder than the baseline, and a drier-than-baseline climate in some western and middle regions over China is depicted in models (Jiang et al., 2013). Jiang et al. (2012) point out the model-data discrepancy over China during the MH, but the lack of seasonal reconstructions in their study limits comparisons with simulations.

An important issue raised by Liu et al. (2014) is that the discrepancy at the annual level could be due to incorrect reconstructions of the seasonal cycle, a key objective in our paper. Moreover, it has been suggested that the vegetation change can strengthen the temperature response in high latitudes (O'Ishi et al., 2009; Otto et al., 2009), as well as alter the hydrological conditions in the tropics (Liu et al., 2007). However, compared to the substantial land cover changes in the MH derived from pollen datasets (Ni et al., 2010; Yu et al., 2000), the changes in vegetation have not yet been fully quantified and discussed in PMIP3 (Taylor et al., 2012).

In this study, for the reconstruction, we firstly used the quantitative method of biomization to reconstruct vegetation types during the MH based on a new synthesis of pollen datasets, and

then used the Inverse Vegetation Model (Guiot et al., 2000; Wu et al., 2007) to obtain the annual, the mean temperature of the warmest month (MTWA) and the mean temperature of the coldest month (MTCO) climate features over China for the MH. In the case of PMIP3 models, we present a comprehensive evaluation of the PMIP3 simulations made with state-of-art climate models using reconstructions of temperature and precipitation. This is the first time that such progress towards a quantitative seasonal climate comparison for the MH over China has been made. This point is crucial because the MH PMIP3 experiment is essentially one that looks at the response of the models to changes in the seasonality of insolation, and the attempt to derive reconstructions of both summer and winter climate to compare with the simulations will thus be able to answer the question posed by Liu et al. (2014) on the importance of seasonal reconstruction.

2. Data and Methodology

2.1 Data

In this study, we collected 159 pollen records, covering most of China, for the MH period (6000±500 ^{14}C yr BP) (Fig. 1). Notably, according to IntCal13 (Reimer et al., 2013), the MH time slice 6000±500 ^{14}C yr BP is about 6800 Cal BP (the average value), which is not totally consistent with the "mid-Holocene" used in CMIP5/PMIP3 experiment (6000 Cal BP). But for a better comparison with BIOME6000 (in which the MH is defined as 6000±500 14C yr BP), we decided to choose the pollen data at 6000±500 14C yr BP in our study. In all 159 records, 65 were from the China Quaternary Pollen Database (CQPD, 2000), three were original datasets obtained in our study, and the others were digitized from pollen diagrams in published papers with a recalculation of pollen percentages based on the total number of terrestrial pollen types. These digitized 91 pollen records were selected according to three criteria: (1) clearly readable pollen diagrams with a reliable chronology with the minimum of three independent age control

123 points since the LGM; (2) including the pollen taxa during 6000±500 ^{14}C yr BP period with a
124 minimum sampling resolution of 1000 years per sample; (3) abandon the pollen records if the
125 published paper mentions the influence of human activity. Based on the digitized pollen
126 assemblages, we use biomization to get the biome scores and biome types. For age control,
127 different dating methods are utilized in the collected pollen records, we applied the CalPal
128 2007 (Weninger et al., 2007) to correct ^{14}C age into calendar age so that they can be
129 contrasted with each other. For lacustrine records, if the specific carbon pool age is mentioned
130 in the literature, the calendar age is corrected after deducting the carbon pool. Otherwise, the
131 influence of carbon pool is not considered. The age-depth model for the pollen records was
132 estimated by linear interpolation between adjacent available dates or by regression. Using
133 ranking schemes from the Cooperative Holocene Mapping Project, the quality of dating
134 control for the mid-Holocene was assessed by assigning a rank from 1 to 7. And 70% of the
135 records used in our study fell into the first and second classes (see Table 1 for detailed
136 information) according to the Webb 1-7 standards (Webb, III T., 1985). Vegetation type was
137 quantitatively reconstructed using biomization (Prentice et al., 1996), following the
138 classification of plant functional types (PFTs) and biome assignment in China by the Members
139 of China Quaternary Pollen Data (CQPD, 2000), which has been widely tested in surface
140 sediment. The new sites (91 digitized data and three original data) added to our database
141 improved the spatial coverage of pollen records, especially in the northwest, the Tibetan
142 Plateau, the Loess Plateau and southern regions, where the data in the previous databases are
143 very limited.

144 Modern monthly mean climate variables, including temperature, precipitation and
145 cloudiness (total cloud fraction), applied in this study, have been collected for each modern
146 pollen site based on the datasets (1951-2001) from 657 meteorological observation stations
147 over China (China Climate Bureau, China Ground Meteorological Record Monthly Report,

1951-2001). The MH soil properties and characteristics used in inverse vegetation model were kept the same with PI conditions, which are derived from the digital world soil map produced by the Food and Agricultural organization (FAO) (FAO, 1995). Atmospheric CO_2 concentration for the MH was taken from ice core records (EPICA community members 2004), and was set at 270 ppmv.

A 3-layer back-propagation (BP) artificial neural network technique (ANN) was used for interpolation on each pollen site (Caudill and Butler, 1992). Five input variables (latitude, longitude, elevation, annual precipitation, annual temperature) and one output variable (biome scores) have been chosen in ANN for the modern vegetation. The ANN has been calibrated on the training set, and its performance has been evaluated on the verification set (20%, randomly extracted from the total sets). After a series of training run, the lowest verification error is obtained with 5 neurons in the hidden layer after 10000 iterations. In our study, at each pollen site, we firstly used the biomization to get the biome scores for both present-day and MH. The anomalies between past (6 ka) and modern vegetation indices (biome scores) was then interpolated to the 0.2×0.2° grid resolution by applying the ANN. After that, the modern grid values are added to the values of the grid of palaeo-anomalies to provide gridded paleo-biome indices. Finally, the biome with the highest index is attributed to each grid point. This ANN method is more efficient than many other techniques on condition that the results are validated by independent data sets, and therefore, it has been widely applied in paleoclimatology (Guiot et al., 1996; Peyron et al., 1998). The schematic diagram of ANN (Figure S1) can be found in Supplementary Information.

2.2 Climate models

PMIP, a long-standing initiative, is a climate-model evaluation project which provides an efficient mechanism for using global climate models to simulate climate anomalies in the past periods and to understand the role of climate feedback. In its third phase (PMIP3), the models

were identical to those used in the Climate Modelling Intercomparison Project 5 (CMIP5) experiments. The experimental set-up for the mid-Holocene simulations in PMIP3 followed the PMIP protocol (Braconnot et al., 2007a, b, 2012). The main forcing between the MH and PI in PMIP3 are the orbital configuration and CH_4 concentration. More precisely, the orbital configuration in the MH climate has an increased summer insolation and a decreased winter insolation in the Northern Hemisphere compared to the PI climate (Berger, 1978). Meantime, the CH_4 concentration is prescribed at 650 ppbv in the MH, while it is set at 760 ppbv in PI (Table 2).

All 13 models (Table 3) from PMIP3 that have the MH simulation have been included in our study, including eight atmosphere-ocean (AO) models and five atmosphere-ocean-vegetation (AOV) models. Means for the last 30 years were calculated from the archived time-series data on individual model grids for climate variables: near surface temperature and precipitation flux, which were bi-linearly interpolated to a uniform 2.5° grid, in order to get the bioclimatic variables (e.g. MAT, MAP, MTWM, MTCO, July precipitation) onto a common grid for comparison with the reconstruction results.

2.3 Vegetation model

The vegetation model, BIOME4 is a coupled bio-geography and biogeochemistry model developed by Kaplan et al. (2003). Monthly mean temperature, precipitation, sunshine percentage (an inverse measure of cloud area fraction), absolute minimum temperature, atmospheric CO_2 concentration and subsidiary information about the soil's physical properties like water retention capacity and percolation rates are the main input variables for the models. It incorporates 13 plant functional types (PFTs), which have different bioclimatic limits. The PFTs are based on physiological attributes and bioclimatic tolerance limits such as heat, moisture and chilling requirements and resistance of plants to cold. These limits determine the areas where the PFTs could grow in a given climate. A viable combination of these PFTs

defines a particular biome among 28 potential options. These 28 biomes can be further classified into 8 megabiomes (Table S1). BIOME4 has been widely utilized to analyze the past, present and potential future vegetation patterns (e.g. Bigelow et al., 2003; Diffenbaugh et al., 2003; Song et al., 2005). In this study, we conducted 13 PI and the MH biome simulations using PIMP3 climate fields (temperature, precipitation and sunshine) as inputs. The climate fields, obtained from PMIP3, are the monthly mean data of the last 30 model years.

2.4 Statistics and interpolation for vegetation distribution

To quantify the differences between simulated (by the climate-model output) and reconstructed (from pollen) between megabiomes, a map-based statistic (point-to-point comparison with observations) called ΔV（Sykes et al., 1999; Ni et al., 2000）was applied to our study. ΔV is based on the relative abundance of different plant life forms (e.g. trees, grass, bare ground) and a series of attributes (e. g. evergreen, needle-leaf, tropical, boreal) for each vegetation class. The definitions and attributes of each plant form follow naturally from the BIOME4 structure and the vegetation attribute values in the ΔV computation were defined for BIOME4 in the same way as for BIOME1（Sykes et al., 1999). The abundance and attribute values are given in Table 4 and Table 5, which describe the typical floristic composition of the biomes. Weighting the attributes is subjective because there is no obvious theoretical basis for assigning relative significance. Transitions between highly dissimilar megabiomes have a weighting of close to 1, whereas transitions between less dissimilar megabiomes are assigned smaller values. The overall dissimilarity between model and data megabiome maps was calculated by averaging the ΔV for the grids with pollen data, while the value was set at 0 for any grid without data. ΔV values < 0.15 can be considered to point to very good agreement between simulated and actual distributions, 0.15-0.30 is good, 0.30-0.45 is fair, 0.45-0.60 is poor, and > 0.80 is very poor (adjusted from Zhang et al., 2010). For spatial pattern comparison,

we compared the simulated vegetation distribution from BIOME4 from each model with the interpolated pattern of reconstruction.

2.5 Inverse vegetation model

Inverse Vegetation Model (Guiot et al., 2000; Wu et al., 2007), highly dependent on the BIOME4 model, is applied to our reconstruction. The key concept of this model can be summarized in two points: firstly, a set of transfer functions able to transform the model output into values directly comparable with pollen data is defined. There is not full compatibility between the biome typology of BIOME4 and the biome typology of pollen data. A transfer matrix (Table S2) was defined in our study where each BIOME4 vegetation type is assigned a vector of values, one of each pollen vegetation type, ranging from 0 (representing an incompatibility between BIOME4 type and pollen biome type) to 15 (corresponding to a maximum compatibility). Secondly, using an iterative approach, a representative set of climate scenarios compatible with the vegetation records is identified among the climate space, constructed by systematically perturbing the input variables (e.g. ΔT, ΔP) of the model (Table S3).

Inverse Vegetation Model (IVM) provides a possibility, for the first time, to reconstruct both annual and seasonal climates for the MH over China. Moreover, it offers a way to consider the impact of CO_2 concentration on competition between PFTs as well as on the relative abundance of taxa, and thus make reconstruction from pollen records more reliable. More detailed information about IVM can be found in Wu et al. (2007).

We applied the inverse model to modern pollen samples to validate the approach by reconstructing the modern climate at each site and comparing it with the observed values. The high correlation coefficients (R=0.75–0.95), intercepts close to 0 (except for the mean temperature of the warmest month), and slopes close to 1 (except for the July precipitation) demonstrated that the inversion method worked well for most variables in China (see Table 6).

2.6 Sensitivity test for vegetation feedback

To quantify the vegetation feedback on climate change during mid-Holocene over China, we did the sensitivity test in CESM version 1.0.5. This version, developed at the National Center for Atmospheric Research, is a widely used coupled model with dynamic atmosphere (CAM4), land (CLM4), ocean (POP2), and sea-ice (CICE4) components (Gent et al., 2011). Here, we use ~2° resolution for the CAM4, configured by ~1.9° (latitude) × 2.5° (longitude) in the horizontal direction and 26 layers in the vertical direction. The POP2 adopts a finer grid, with a nominal 1° horizontal resolutions and 60 layers in the vertical direction. The land and sea-ice components have the same horizontal grids as the atmosphere and ocean components, respectively.

Two experiments were conducted, including a mid-Holocene (MH) experiment (6 ka) with original vegetation setting (prescribed as PI vegetation for MH) and a MH experiment with reconstructed vegetation (6 ka_VEG). In detail, experiment 6 ka used the MH orbital parameters (Eccentricity=0.018682; Obliquity=24.105°; Angular precession=0.87°) and modern vegetation (Salzmann et al., 2008). Compared to experiment 6 ka, experiment 6 ka_VEG used our reconstructed vegetation in China. Except for the changed vegetation, all other boundary conditions were kept unchanged in these two experiments, including the solar constant (1365 W m^{-2}), modern topography and ice sheet, and pre-industrial greenhouse gases (CO_2 = 280 ppmv; CH_4 = 760 ppbv; N_2O = 270 ppbv). Experiment 6 ka was initiated from the default pre-industrial simulation and run for 500 model years. Experiment 6 ka_VEG was initiated from model year 301 of experiment 6 ka and run for another 200 model years. We analyzed the computed climatological means of the last 50 model years from each experiment here.

3. Results

3.1 Comparison of annual and seasonal climate changes at the MH

In this study, we collected 159 pollen records, broadly covering the whole of China (Fig. 1). To check the reliability of the collected data, we first categorized our pollen records into megabiomes in line with the standard tables developed for the BIOME6000 (Table S1), and compared them with the BIOME6000 dataset (Fig.2). The match between collected data and the BIOME6000 is more than 90% (145 out of 159 sites) for both the MH and PI.

Based on pollen records, the spatial pattern of climate changes over China during the MH, deduced from IVM, are presented in Fig. 3 (left panel, points), alongside the results from PMIP3 models (shaded in Fig. 3). For temperature, a warmer-than-present annual climate condition (~0.7 K on average) is derived from pollen data (the points in Fig. 3a), with the largest increase occurring in the northeast (3-5 K) and a decrease in the northwest and on Tibetan Plateau. On the other hand, the results from a multi-model ensemble (MME) indicate a colder annual temperature generally (~-0.4 K on average), with significant cooling in the south and slight warming in the northeast (shaded in Fig. 3a). Of the 13 models, 11 simulate a cooler annual temperature compared with PI as MME. However, two models (HadeGEM2-ES and CNRM-CM5) present the same warmer condition as was found in the reconstruction (Fig. 3d). Compared to the reconstruction, the annual mean temperature during the MH is largely underestimated by most PMIP3 models, which depict an anomaly ranging from ~-1 to ~0.5 K. Concerning seasonal change, during the MH, MTWA from the data is ~0.5 K higher than PI, with the largest increase in the northeast and a decrease in the northwest. From model outputs, an average increase of ~1.2 K is reproduced by MME, with a more pronounced warming at high latitudes which is consistent with the insolation change (Berger, 1978). Fig. 3e shows that all 13 models reproduce the same warmer summer temperatures as the data, and that HadGEM2-ES

and CNRM-CM5, reproduce the largest increases among the models. Although the warmer MTWA is consistent between the models and data, there is a discrepancy between them on MTCO. In Fig. 3c, the data show an overall increase of ~1 K, with the largest increase occurring in the northeast and a decrease of opposite magnitude on the Tibetan Plateau. Inversely, MME reproduces a decreased MTCO with an average amplitude of ~-1.3 K, the coolest areas being the southeast, the Loess Plateau and the northwest. Similarly to the MME, all 13 models simulate a colder-than-present climate with amplitudes ranging from ~-2.0 K (CCSM4 and FGOALS-g2) to ~-0.7 K (HadGEM2-ES and CNRM-CM5).

Concerning annual change in precipitation, the reconstruction shows wetter conditions during the MH across almost the whole of China with the exception of part of the northwest. The southeast presents the largest increase in annual precipitation. All but 2 models (MIROC-ESM and FGOALS-g2) depict wetter conditions with an amplitude of ~10 mm to ~50 mm. The reconstruction and MME results also indicate an increased annual precipitation during MH (Fig.4a), with a much larger magnitude visible in the reconstruction (~30 mm, ~230 mm respectively). The main discrepancy in annual precipitation between simulations and reconstruction occurs in the northeast, which is depicted as drier by the models and wetter by the data. With regard to seasonal change, the reconstruction shows an overall increase in July rainfall (~50 mm on average), with a decrease in the northwestern regions and East Monsoon region at Yangtze River valley. In line with the reconstruction, the MME also shows an overall increase in rainfall (~7 mm on average), with a decrease in the northwest for July (Fig.4b). Notably, a much larger increase is simulated for the south and the Tibetan Plateau by the models, while the opposite pattern emerges along the eastern margin from both models and data. For January precipitation, the reconstruction shows an overall increase in most region (~15 mm), except for the northwestern region, while MME indicates a slight decrease (~3 mm on

317 average). More detailed information about the geographic distribution of simulated temperature
318 and precipitation for each model can be found in Fig. S2-S7.

319 Table S4 provides the biome score from IVM for pollen data collected from published papers.
320 The reconstructed climate change derived from IVM at each pollen site can be found in Table
321 S5, in which the columns show the median and the 90% interval (5th to 95th percentage) for
322 feasible climate values produced with the IVM approach. The simulated values for each of the
323 climate variables as shown in the boxplots (Figure 3 and Figure 4) are given in the Table S6
324 and Table S7.

325 **3.2 Comparison of vegetation change at the MH**

326 The use of the PMIP3 database is clearly limited by the different vegetation inputs among the
327 models for the MH period (Table S8). Only HadGEM2-ES and HadGEM2-CC use a dynamic
328 vegetation for the MH, and the other 11 models are prescribed to PI with or without interactive
329 LAI, which would introduce a bias to the role of vegetation-atmosphere interaction in the MH
330 climates. To evaluate the model results against the reconstruction for the MH vegetation, we
331 conducted 13 biome simulations in BIOME4 using PIMP3 climate fields, and the megabiome
332 distribution for each model during the MH is displayed in Fig. 5 (see Fig. S8 for PI vegetation
333 comparison). To quantify the model-data dissimilarity between megabiomes, a map-based
334 statistic called ΔV (Sykes et al., 1999; Ni et al., 2000) was applied here (detailed information is
335 in the methodology section).

336 Fig. S9 shows the dissimilarity between simulations and observations for megabiomes
337 during the MH, with the overall values for ΔV ranging from 0.43 (HadGEM2-ES) to 0.55
338 (IPSL-CM5A-LR). According to the classification of ΔV (see in the methodology section) for
339 the 13 models, 12 (all except HadGEM2-ES) showed poor agreement with the observed
340 vegetation distribution. Most models poorly simulate the desert, grassland and tropical forest

areas for both periods, but perform better for warm mixed forest, tundra and temperate forest. However, this statistic is based on a point-to-point comparison and so the ΔV calculated here cannot represent an estimation of full vegetation simulation due to the uneven distribution of pollen data and the potentially huge difference in area of each megabiome. For instance, tundra in our data for PI is represented by only 4 points, which counts for a small contribution to the ΔV since we averaged it over a total of 159 points, but this calculation could induce a significant bias if these 4 points cover a large area of China.

So, we used the biome scores based on the artificial neural network technique as described by Guiot et al. (1996) for interpolation (the plots in red rectangle in Fig. 5), and compared the simulated vegetation distribution from BIOME4 for each model with the interpolated pattern. During the MH, most models are able to capture the tundra on the Tibetan Plateau as well as the combination of warm mixed forest and temperate forest in the southeast. However, all models fail to simulate or underestimate the desert area in the northwest compared to reconstructed data. The main model-data inconsistency in the MH vegetation distribution occurs in the northeast, where data show a mix of grassland and temperate forest, and the models show a mix of grassland and boreal forest.

The area statistic carried out for simulated vegetation changes (Fig. 6) reveals that the main difference during the MH, compared with PI, is that grassland replaced boreal forest in large tracts of the northeast (Fig. 5, Fig. S8). No other significant difference in vegetation distribution between the two periods was derived from models. Unlike in models, three main changes in megabiomes during the MH are depicted by the data. Firstly, the megabiomes converted from grassland to temperate forest in the northeast. Secondly, a large area of temperate forest was replaced in the southeast by a northward expansion of warm mixed forest. Thirdly, in the northwest and at the northern margin of the Tibetan Plateau, part of the desert area changed into grassland. However, none of the models succeed in capturing these features, especially the

transition from grassland into forest in the northeast during the MH. Therefore, this failure to capture vegetation changes between the two periods will lead to a cumulating inconsistency in the model-data comparison for climate anomalies because of the vegetation-climate feedbacks.

4. Discussion

4.1 Validation and uncertainties for reconstruction

To investigate the discrepancy between model-data for the MH climate change over China, the reliability of our reconstruction should be firstly considered. For the cross-proxy validation, we compared our reconstruction with previous studies concerning the MH climate change over China based on multiple proxies (including pollen, lake core, palaeosol, ice core, peat and stalagmite), the related references and detailed information are listed in Supplementary Information (Table S9 and Table S10). In comparison with PI condition, most reconstructions reproduced warmer and wetter annual condition during the MH (Fig. 7), same as our study. In other words, this discrepancy between model-data for climate change over China during the MH is common and robust in reconstructions derived from different proxies. Our study just reinforces the picture given by the discrepancies between PMIP simulation and pollen data derived from a synthesis of the literature.

However, there are still some bias in the reconstruction. Estimated climates for the present day from IVM were compared with observed climates (Table 6), the slopes and intercepts show slightly bias for annual and January precipitation, while there is considerable bias between IVM reconstruction and observation for temperature and July precipitation. For the uncertainties on data reconstruction, IVM relies heavily on BIOME4, and since BIOME4 is a global vegetation model, it is possible that the spatial robustness of regional reconstruction could be less than that of global reconstruction due to the failure in simulating local features (Bartlein et al., 2011). Moreover, the output of the model is not directly compared to the pollen data, the conversion

of BIOME4 biomes to pollen biomes by the transfer matrix may add the source of uncertainty in reconstruction. All these bias in reconstruction should be considered in the discrepancy between model-data for climate change during the MH over China.

4.2 Uncertainties for simulation

The discrepancies between model-data for MH climate change could also be resulted from the uncertainties in simulation. Firstly, the coarse spatial resolution of models. Previous study shows the GCMs from PMIP3 is reliable to simulate the geographical distribution of temperature and precipitation over China for present day without downscaling, but there is considerable bias between simulation and observation for precipitation (Jiang et al., 2016). In particular, the climate fields, directly used from the model output without downscaling, will not contain the spatial variability of modern climate that in topographically complex areas. And thus, it's necessary to check in which degree the model-data mismatch is related to rough topography used in the climate models. In PMIP3, MRI-CGCM3 has the highest resolution (Atmosphere: 320*160*L48; Ocean: 364*368*L51), while IPSL-CM5A-LR has the lowest one (Atmosphere: 96*96*L39; Ocean: 182*149*L31). In Fig. 8, we give the actual modern topography and the interpolated topography used in MRI-CGCM3 and IPSL-CM5A-LR. For MRI-CGCM3, the topography is very close to the observation, so for this model, the model-data discrepancy during MH over China is not related to the resolution. However, for the model with coarse resolution (IPSL-CM5A-LR), it's true that the coarse version of model will lead to bias in topography when the regional diversity is discussed. The variations in topography could influence the vegetation and hence the simulated climate. To quantify this impact, we compare the topography and PI climate results of IPSL-CM5A-LR and IPSL-CM5A-MR. Fig. 9 shows that the difference in topography caused by model resolution do has an impact on small scales (e.g. south region of the Tibetan Plateau), but not on the

414 overall pattern. For a better comparison, the climate variables should be downscaled in the
415 future work.

416 Secondly, besides the qualitative consistency among models, caused by the protocol of
417 PMIP3 experiments (Table 2), a variability in the magnitude of anomalies between models is
418 clearly illustrated by the boxplots (Fig.3 and Fig.4), especially for the temperature anomaly. Fig.
419 S10 demonstrates that there is no any clear relationship between PI temperature and
420 temperature anomaly (MH-PI). In other words, these disparities in value or even pattern among
421 models are not resulted from the difference in PI simulation, instead, they reflect the obvious
422 differences in the response by the climate models to the MH forcing which raises on the
423 question of the magnitude of feedbacks among models.

424 As positive feedbacks between climate and vegetation are important to explain regional
425 climate changes, the failure to capture or the underestimation of the amplitude and pattern of
426 the observed vegetation differences among models (see Section 3.2) could amplify and partly
427 account for the model-data disparities in climate change, mainly due to variations in the albedo.
428 Because the HadGEM2-ES and HadGEM2-CC are the only two models in PMIP3 with
429 dynamic vegetation simulation for the MH, we thus focused on them to examine the variations
430 in vegetation fraction in the simulations. The main vegetation changes during the MH
431 demonstrated by HadGEM2-ES are increased tree coverage (~15%) and a decreased bare soil
432 fraction (~6%), while HadGEM2-CC depicts a ~3% decrease in tree fraction and a ~1%
433 increase in bare soil (Fig. S11). We made a rough calculation of albedo variance caused solely
434 by vegetation change for both two models and for our reconstruction, based on the area fraction
435 and albedo value of each vegetation type (Betts, 2000; Bonfils et al., 2001; Oguntunde et al.,
436 2006; Bonan, 2008).

437 The overall albedo change from the vegetation reconstruction during the MH shows a ~1.8%
438 decrease when snow-free, with a much larger impact (~4.2% decrease) when snow-covered.
439 The results from HadGEM2-ES are highly consistent with the albedo changes from the
440 reconstruction, featuring a ~1.4% (~6.5%) decrease without (with) snow, while HadGEM2-CC
441 produces an increased albedo value during the MH (~0.22% for snow-free, ~1.9% with
442 snow-cover), depending on its vegetation simulation. Two ideas could be inferred from this
443 calculation, 1) HadGEM2-ES is much better in simulating the MH vegetation changes than
444 HadGEM2-CC. 2) the failure by models to capture these vegetation changes will result in a
445 much larger impact on winter albedo (with snow) than summer albedo (without snow). In
446 conclusion, there is an obvious advantage of using AOVGCM instead of AOGCM when we
447 discussing about the MH climate, but the premise is that the AOVGCM can simulate accurate
448 vegetation distribution.

449 These surface albedo changes due to vegetation changes could have a cumulative effect on
450 the regional climate by modifying the radiative fluxes. For instance, the spread of trees into the
451 grassland biome in the northeast during the MH, revealed by the reconstruction in our study,
452 should act as a positive feedback to climate warming by increasing the surface net shortwave
453 radiation associated with reductions in albedo due to taller and darker canopies (Chapin et al.,
454 2005). Previous studies show that cloud and surface albedo feedbacks on radiation are major
455 drivers of differences between model outputs for past climates. Moreover, the land surface
456 feedback shows large disparities among models (Braconnot and Kageyama, 2015).

457 We used a simplified approach (Taylor et al., 2007) to quantify the feedbacks and to compare
458 model behavior for the MH, thus justifying the focus on surface albedo and atmospheric
459 scattering (mainly accounting for cloud change). Surface albedo and cloud change are
460 calculated using the simulated incoming and outgoing radiative fluxes at the Earth's surface
461 and at the top of atmosphere (TOA), based on data for the last 30 years averaged from all

462 models. Using this framework, we quantified the effect of changes in albedo on the net
463 shortwave flux at TOA (Braconnot and Kageyama, 2015), and further investigated the
464 relationship between these changes and temperature change. Fig.10 shows that most models
465 produced a negative cloud cover and surface albedo feedback on the annual mean shortwave
466 radiative forcing. Concerning seasonal change, the shortwave cloud and surface feedback in
467 most models tend to counteract the insolation forcing during the boreal summer, while they
468 enhance the solar forcing during winter. A strong positive correlation between albedo feedback
469 and temperature change is depicted, with a large spread in the models owing to the difference in
470 albedo in the 13 models. In particular, CNRM-CM5 and HadGEM2-ES capture higher values
471 of cloud and surface albedo feedback, which could be the reason for the reversal of the
472 decreased annual temperature seen in other models (Fig. 3d).

473 However, the vegetation patterns produced by BIOME4 in Figure 5 are not used in PMIP3
474 experiment setup, it's actually determined by the input variables from models. Therefore, the
475 disagreements of MH vegetation pattern possibly are inherited from the PI. To better quantify
476 the vegetation-climate feedback, two experiments were conducted in CESM version 1.0.5,
477 including a mid-Holocene (MH) experiment (6 ka) with original vegetation setting
478 (prescribed as PI vegetation for the MH) and a MH experiment with reconstructed vegetation
479 (6 ka_VEG). Fig. 11 shows the climate anomalies (6 ka_VEG minus 6 ka) between two
480 simulations, for both annual and seasonal scale. For temperature, it's clear that the 6 ka_VEG
481 simulation reproduces a warmer annual mean climate (~0.3 K on average) as well as an
482 obviously warmer winter (~0.6 K on average). For precipitation, the reconstructed vegetation
483 leads to more annual and seasonal precipitation, which can also reconcile the discrepancy of
484 increase amplitude for precipitation during the MH between model-data (data reproduced
485 larger amplitude than model, revealed by our study). So the mismatch between model-data in
486 MH vegetation could partly account for the discrepancy of climate due to the interaction

between vegetation and climate through radiative and hydrological forcing with albedo. These results pinpoint the value of building a new generation of models able to capture not only the atmosphere and ocean response, but also the non-linear responses of vegetation and hydrology to the climate change.

5. Conclusion

In this study, we compare the annual and seasonal outputs from the PMIP3 models with an updated synthesis of climate reconstruction over China, including, for the first time, a seasonal cycle of temperature and precipitation. In response to the seasonal insolation change prescribed in PMIP3 for the MH, all models produce similar large-scale patterns for seasonal temperature and precipitation (higher than present July precipitation and MTWA, lower than present MTCO), with either an over- or underestimate of the climate changes when compared to the data. The main discrepancy emerging from the model-data comparison occurs in the annual and MTCO, where data show an increased value and most models simulate the opposite except CNRM-CM5 and HadGEM2-ES reproduced the higher-than-present annual temperature during MH as data showed. By conducting simulations in BIOME4 and CESM, we show that the surface processes are the key factors drawing the uncertainties between models and data. These results pinpoint the crucial importance of including the non-linear responses of the surface water and energy balance to vegetation changes. However, it should also be noted that prescribing the vegetation with reconstructed biomes would reduce the power of the biome-based climate reconstruction, owing to the potential circularity (prescribe the vegetation to get the vegetation). Moreover, besides the vegetation influence, to which extent this model-data discrepancy is related to rough topography, soil type and other possible factors should be investigated in the future work.

Data availability

The PMIP3 output is publicly available at website (http://pmip3.lsce.ipsl.fr/) by the climate modelling groups, the 65 pollen biomization results are provided by Members of China Quaternary Pollen Data Base (CQPD), Table 1 shows the information (including references) of the 91 collected pollen records and 3 original ones in our study, the biome scores of these 94 pollen records derived from IVM are listed in Table S4. All the reconstructed climate values at each pollen site from IVM are provided in Table S5. For the data from CQPD, the basic information (location, data supporter, age control and biome type of each site) can be found in CQPD (2000), while the original data are not publicly available yet. To whom request for the data, you can contact with Yunli Luo (lyl@ibcas.ac.cn, Institute of Botany, Chinese Academy of Sciences, Beijing, 100093, China), a core member and academic secretary of the CQPD.

Author contribution

Yating Lin carried out the model-data analysis and prepared for the first manuscript, Gilles Ramstein contributed a lot to the paper's structure and content, Haibin Wu provided the reconstruction results from IVM and contributed the paper's structure and content. Raj Rani-Singh conducted the BIOME4 simulations. Ran Zhang carried out the simulation in CESM. Pascale Braconnot, Masa Kegeyama and Zhengtang Guo contributed great ideas on model-data comparison work. Qin Li and Yunli Luo provided pollen data. All co-authors helped to improve the paper.

Competing interest

The authors declare no competing interests.

Acknowledgements

We acknowledge the World Climate Research Program's Working Group on Coupled Modelling, which is responsible for PMIP/CMIP, and we thank the climate modelling groups for producing and making available their model output. We are grateful to Marie-France Loutre, Patrick Bartlein and three anonymous reviewers for constructive comments. This research was funded by the National Basic Research Program of China (Grant no. 2016YFA0600504), the National Natural Science Foundation of China (Grant nos. 41572165, 41690114, and 41125011), the Sino-French Caiyuanpei Program, and the Bairen Programs of the Chinese Academy of Sciences.

References

An, C., Zhao, J., Tao, S., Lv, Y., Dong, W., Li, H., Jin, M., and Wang, Z.: Dust variation recorded by lacustrine sediments from arid Central Asia since ~ 15 cal ka BP and its implication for atmospheric circulation, Quaternary Research, 75, 566-573, 2011.

Bao, Q., Lin, P., Zhou, T., Liu, Y., Yu, Y., Wu, G., He, B., He, J., Li, L., Li, J., Li, Y., Liu, H., Qiao, F., Song, Z., Wang, B., Wang, J., Wang, P., Wang, X., Wang, Z., Wu, B., Wu, T., Xu, Y., Yu, H., Zhao, W., Zheng, W., and Zhou, L.: The flexible global ocean-atmosphere-land system model, spectral version 2: FGOALS-s2. Advances in Atmospheric Sciences, 30, 561-576, 2013.

Bartlein, P. J., Harrison, S. P., Brewer, S., Connor, S., Davis, B. A. S., Gajewski, K., Guiot, J., Harrison-Prentice, T. I., Henderson, A., Peyron, O., Prentice, I. C., Scholze, M., Seppä, H., Shuman, B., Sugita, S., Thompson, R. S., Viau, A. E., Williams, J., and Wu, H.B.: Pollen-based continental climate reconstructions at 6 and 21ka: a global synthesis, Climate Dynamics, 37, 775-802, 2011.

557 Berger, A.: Long-Term Variations of Daily Insolation and Quaternary Climatic Changes,
558 Journal of the Atmospheric Sciences, 35, 2362-2367, 1978.

559 Betts, R. A.: Offset of the potential carbon sink from boreal forestation by decreases in surface
560 albedo, Nature, 408, 187-190, 2000.

561 Bigelow, N. H., Brubaker, L. B., Edwards, M. E., Harrison, S. P., Prentice, I. C., Anderson, P.
562 M., Andreev, A. A., Bartlein, P. J., Christensen, T. R., Cramer, W., Kaplan, J. O., Lozhkin,
563 A. V., Matveyeva, N. V., Murray, D. F., David McGuire, A., Razzhivin, V. Y., Ritchie, J. C.,
564 Smith, B., Walker, A. D., Gajewski, K., Wolf, V., Holmqvist, B. H., Igarashi, Y.,
565 Kremenetskii, K., Paus, A., Pisaric, M. F. J., and Volkova, V. S.: Climate change and Arctic
566 ecosystems: 1. Vegetation changes north of 55°N between the last glacial maximum,
567 mid-Holocene and present, Journal of Geophysical Research, 108, 1-25, 2003.

568 Bonan, G. B.: Forests and Climate Change: Forcings, Feedbacks, and the Climate Benefits of
569 Forests, Science, 320, 1444-1449, 2008.

570 Bonfils, C., de Noblet-Ducoudré, N, Braconnot, P., and Joussaume, S.: Hot Desert Albedo and
571 Climate Change: Mid-Holocene Monsoon in North Africa, Journal of Climate, 14,
572 3724–3737, 2001.

573 Braconnot, P., and Kageyama, M.: Shortwave forcing and feedbacks in Last Glacial Maximum
574 and Mid-Holocene PMIP3 simulations, Philosophical Transactions of the Royal Society A:
575 Mathematical, Physical and Engineering Sciences, 373, 2054-2060, 2015.

576 Braconnot, P., Harrison, S. P., Kageyama, M., Bartlein, P. J., Masson-Delmotte, V., Abe-Ouchi,
577 A., Otto-Bliesner, B., and Zhao, Y.: Evaluation of climate models using palaeoclimatic data:
578 Nature Climate Change, 2, 417-421, 2012.

579 Braconnot, P., Otto-Bliesner, B., Harrison, S., Joussaume, S., Peterchmitt, J. Y., Abe-Ouchi, A.,
580 Crucifix, M., Driesschaert, E., Fichefet, T., Hewitt, C. D., Kageyama, M., Kitoh, A., Laine,
581 A., Loutre, M. F., Marti, O., Merkel, U., Ramstein, G., Valdes, P., Weber, S. L., Yu, Y., and
582 Zhao, Y.: Results of PMIP2 coupled simulations of the Mid-Holocene and Last Glacial
583 Maximum-Part 1: experiments and large-scale features, Climate of the Past, 3, 261-277,
584 2007a.

585 Braconnot, P., Otto-Bliesner, B., Harrison, S., Joussaume, S., Peterschmitt, J. Y., Abe-Ouchi,
586 A., Crucifix, M., Driesschaert, E., Fichefet, T., Hewitt, C. D., Kageyama, M., Kitoh, A.,
587 Loutre, M. F., Marti, O., Merkel, U., Ramstein, G., Valdes, P., Weber, L., Yu, Y., and Zhao,
588 Y.: Results of PMIP2 coupled simulations of the Mid-Holocene and Last Glacial
589 Maximum-Part 2: feedbacks with emphasis on the location of the ITCZ and mid- and high
590 latitudes heat budget, Climate of the Past, 3, 279-296, 2007b.

591 Cai, Y.: Study on environmental change in Zoige Plateau: Evidence from the vegetation
592 record since 24000a B.P., Chinese Academy of Geological Sciences, Mater Dissertation,
593 2008 (in Chinese with English abstract).

594 Caudill, M., Bulter, C.: Understanding Neural Networks, Basic Networks, 1, 309, 1992.

595 Chapin, F. S., Sturm, M., Serreze, M. C., McFadden, J. P., Key, J. R., Lloyd, A. H.,
596 McGuire, A. D., Rupp, T. S., Lynch, A. H., Schimel, J. P., Beringer, J., Chapman, W. L.,
597 Epstein, H. E., Euskirchen, E. S., Hinzman, L. D., Jia, G., Ping, C.L., Tape, K. D.,
598 Thompson, C. D. C., Walker, D. A., and Welker, J. M.: Role of Land-Surface Changes in
599 Arctic Summer Warming, Science, 310, 657-660, 2005.

600 Chen, F., Cheng, B., Zhao, Y., Zhu, Y., and Madsen, D. B.: Holocene environmental change
601 inferred from a high-resolution pollen record, Lake Zhuyeze, arid China, The Holocene, 16,
602 675-684, 2006.

603 Chen, F., Xu, Q., Chen, J., Birks, H. J. B., Liu, J., Zhang, S., Jin, L., An, C., Telford, R. J., Cao,
604 X., Wang, Z., Zhang, X., Selvaraj, K., Lu, H., Li, Y., Zheng, Z., Wang, H., Zhou, A., Dong,
605 G., Zhang, J., Huang, X., Bloemendal, J., and Rao, Z.: East Asian summer monsoon
606 precipitation variability since the last deglaciation, Scientific Reports, 5, 1-11, 2015.

607 Cheng, B., Chen, F., and Zhang, J.: Palaeovegetational and Palaeoenvironmental Changes in
608 Gonghe Basin since Last Deglaciation, Acta Geographica Sinica, 11, 1336-1344, 2010 (in
609 Chinese with English abstract).

610 Cheng, H., Edwards, R. L., Sinha, A., Spötl, C., Yi, L., Chen, S., Kelly, M., Kathayat, G., Wang,
611 X., Li, X., Kong, X., Wang, Y., Ning, Y., and Zhang, H.: The Asian monsoon over the past
612 640,000 years and ice age terminations, Nature, 534, 640, 2016.

613 Cheng, Y.: Vegetation and climate change in the north-central part of the Loess Plateau since
614 26,000 years, China University of Geosciences, Master Dissertation, 2011 (in Chinese
615 with English abstract).

616 Collins, W. J., Bellouin, N., Doutriaux-Boucher, M., Gedney. N., Halloran, P., Hinton, T.,
617 Hughes, J., Jones, C.D., Joshi, M., Liddicoat, S., Martin, G., O'Connor, F., Rae, J., Senior,
618 C., Sitch, S., Totterdell, I., Wiltshire, A., and Woodward, S.: Development and evaluation
619 of an Earth-system model—HadGEM2, Geoscientific Model Development, 4, 1051–1075,
620 2011.

621 Cui, M., Luo, Y., and Sun, X.: Paleovegetational and paleoclimatic changed in Ha'ni Lake,
622 Jilin since 5ka BP, Marine Geology & Quaternary Geology, 26, 117-122, 2006 (in
623 Chinese with English abstract).

624 Dallmeyer, A., Claussen, M., Ni, J., Cao, X., Wang, Y., Fischer, N., Pfeiffer, M., Jin, L.,
625 Khon, V., Wagner, S., Haberkorn, K., and Herzschuh, U.: Biome changes in Asia cinse

626 the mid-Holocene-and analysis of difference transient Earth system model simulations,
627 Climate of the Past, 13, 107-134, 2017.

628 Davis, B. A. S., Brewer, S., Stevenson, A. C., and Guiot, J.: The temperature of Europe during
629 the Holocene reconstructed from pollen data, Quaternary Science Reviews, 22, 1701-1716,
630 2003.

631 Diffenbaugh, N.S., Sloan, L.C., Snyder, M.A., Bell, J.L., Kaplan, J., Shafer, S.L., and Bartlein,
632 P.J.: Vegetation sensitivity to global anthropogenic carbon dioxide emissions in a
633 topographically complex region, Global Biogeochemical Cycles, 17, 1067,
634 doi:10.1029/2002GB001974, 2003.

635 Dufresne, J.L., Foujols, M.A., Denvil, S., Caubel, A., Marti, O., Aumont, O., Balkanski, Y.,
636 Bekki, S., Bellenger, H., Benshila, R., Bony, S., Bopp, L., Braconnot, P., Brockmann, P.,
637 Cadule, P., Cheruy, F., Codron, F., Cozic, A., Cugnet, D., Noblet, N., Duvel, J.P., Ethe, C.,
638 Fairhead, L., Fichefet, T., Flavoni, S., Friedlingstein, P., Grandpeix, J.Y., Guez, L.,
639 Guilyardi, E., Hauglustaine, D., Hourdin, F., Idelkadi, A., Ghattas, J., Joussaume, S.,
640 Kageyama, M., Krinner, G., Labetoulle, S., Lahellec, A., Lefevre, M.-F., Lefevre, F.,
641 Levy, C., Li, Z.X., Lloyd, J., Lott, F., Madec, G., Mancip, M., Marchand, M., Masson, S.,
642 Meurdesoif, Y., Mignot, J., Musat, I., Parouty, S., Polcher, J., Rio, C., Schulz, M.,
643 Swingedouw, D., Szopa, S., Talandier, C., Terray, P., Viovy, N., and Vuichard, N.:
644 Climate change projections using the IPSL-CM5 Earth system model: from CMIP3 to
645 CMIP5, Climate Dynamics, 40, 2123-2165, 2013.

646 EPICA Community Members: Eight glacial cycles from an Antarctic ice core, Nature, 429,
647 623-628, 2004.

648 Food and Agricultural organization: Soil Map of the World 1:5000,000. 1995.

649 Farrera, I., Harrison, S. P., Prentice, I. C., Ramstein, G., Guiot, J., Bartlein, P. J., Bonnefille, R.,
650 Bush, M., Cramer, W., von Grafenstein, U., Holmgren, K., Hooghiemstra, H., Hope, G.,
651 Jolly, D., Lauritzen, S. E., Ono, Y., Pinot, S., Stute, M., and Yu, G.: Tropical climates at the
652 Last Glacial Maximum: a new synthesis of terrestrial palaeoclimate data. I. Vegetation,
653 lake-levels and geochemistry, Climate Dynamics, 15, 823-856, 1999.

654 Fischer, N., and Jungclaus, J. H.: Evolution of the seasonal temperature cycle in a transient
655 Holocene simulation: orbital forcing and sea-ice, Climate of the Past, 7, 1139-1148, 2011.

656 Ganopolski, A., Kubatzki, C., Claussen, M., Brovkin, V., and Petoukhov, V.: The Influence of
657 Vegetation-Atmosphere-Ocean Interaction on Climate during the Mid-Holocene, Science,
658 280, 1916-1919, 1998.

659 Gent, P.R., Danabasoglu, G., Donner, L.J., Holland, M.M., Hunke, E.C., Jayne, S.R.,
660 Lawrence, D.M., Neale, R.B., Rasch, P.J., Vertenstein, M., Worley, P.H., Yang, Z., and
661 Zhang, M.: The community climate system model version 4, Journal of Climate, 24,
662 4973-4991, 2011.

663 Giorgetta, M.A., Jungclaus, J., Reick, C.H., Legutke, S., Bader, J., Bottinger, M., Brovkin, V.,
664 Crueger, T., Esch, M., Fieg, K., Glushak, K., Gayler, V., Haak, H., Hollweg, H.D., Ilyina,
665 T., Kinne, S., Kornblueh, L., Matei, D., Mauritsen, T., Mikolajewicz, U., Mueller, W.,
666 Notz, D., Pithan, F., Raddatz, T.J., Rast, S., Redler, R., Roeckner, E., Schmidt, H., Schnur,
667 R., Segschneider, J., Six, K.D., Stockhause, M., Timmreck, C., Wegner, J., Widmann, H.,
668 Wieners, K.H., Claussen, M., Marotzke, J., and Stevens, B.: Climate and carbon cycle
669 changes from 1850 to 2100 in MPI-ESM simulations for the Coupled Model
670 Intercomparison Project phase 5, Journal of Advances in Modeling Earth System, 5,
671 572-597, 2013.

672 Gong, X.: High-resolution paleovegetation reconstruction from pollen in Jiachuanyuan, Baoji,
673 Capital Normal University, Master Dissertation, 2006 (in Chinese with English abstract).

674 Guiot, J., and Goeury, C.: PPPBASE, a software for statistical analysis of paleoecological and
675 paleoclimatological data, Dendrochronologia, 14, 295-300, 1996.

676 Guiot, J., Harrison, S., and Prentice, I. C.: Reconstruction of Holocene precipitation patterns in
677 Europe using pollen and lake level data, Quaternary Research, 40, 139-149, 1993.

678 Guiot, J., Torre, F., Jolly, D., Peyron, O., Boreux, J. J., and Cheddadi, R.: Inverse vegetation
679 modeling by Monte Carlo sampling to reconstruct palaeoclimates under changed
680 precipitation seasonality and CO_2 conditions: application to glacial climate in
681 Mediterranean region, Ecological Modelling, 127, 119-140, 2000.

682 Guo, L., Feng, Z., Lee, X., Liu, L., and Wang, L.: Holocene climatic and environmental
683 changes recorded in Baahar Nuur Lake in the Ordos Plateau, Southern Mongolia of china,
684 Chinese Science Bulletin, 52, 959-966, 2007.

685 Hargreaves, J. C., Annan, J. D., Ohgaito, R., Paul, A., and Abe-Ouchi, A.: Skill and reliability
686 of climate model ensembles at the Last Glacial Maximum and mid-Holocene, Climate of
687 the Past, 9, 811-823, 2013.

688 Harrison, S. P., Bartlein, P. J., Brewer, S., Prentice, I. C., Boyd, M., Hessler, I., Holmgren, K.,
689 Izumi, K., and Willis, K.: Climate model benchmarking with glacial and mid-Holocene
690 climates, Climate Dynamics, 43, 671-688, 2014.

691 Harrison, S. P., Bartlein, P. J., K., Izumi, Li, G., Annan, J., Hargreaves, J., Braconnot, P., and
692 Kageyama, M.: Evaluation of CMIP5 paleo-simulations to improve climate projections,
693 Nature Climate Change, 5, 735-743, 2015.

694 Harrison, S., P., Braconnot, P., Hewitt, C., and Stouffer, R., J.: Fourth International Workshop
695 of the Palaeoclimate Modelling Intercomparison Project (PMIP): Lauching PMIP2 Phase II,
696 EOS, 83, 447-457, 2002.

697 Herzschuh, U., Kramer, A., Mischke, S., and Zhang, C.: Quantitative climate and vegetation
698 trends since the late glacial on the northeastern Tibetan Plateau deduced from Koucha
699 Lake pollen spectra, Quaternary Research, 71, 162-171, 2009.

700 Herzschuh, U., Kürschner, H., and Mischke, S.: Temperature variability and vertical
701 vegetation belt shifts during the last ~50,000 yr in the Qilian mountains (NE margin of
702 the Tibetan Plateau, China), Quaternary Research, 66, 133-146, 2006.

703 Huang, C., Elis, V. C., and Li, S.: Holocene environmental changes of Western and Northern
704 Qinghai-Xizang Plateau Based on pollen analysis, Acta Micropalaeontologica Sinica, 4,
705 423-432, 1996 (in Chinese with English abstract).

706 Jeffrey, S.J., Rotstayn, L.D., Collier, M., Dravitzki, S.M., Hamalainen, C., Moeseneder, C.,
707 Wong, K.K., and Syktus, J.I.: Australia' s CMIP5 submission using the CSIRO-Mk3.6
708 model, Australian Meteorological and Oceanographic Journal, 63, 1-13, 2013.

709 Jia, L., and Zhang, Y.: Studies on Palynological assemblages and paleoenvironment of late
710 Quaternary on the east margin of the Chanjiang (Yangtze) river delta, Acta
711 Micropalaeontologica Sinica, 23, 70-76, 2006 (in Chinese with English abstract).

712 Jiang, D., Lang, X., Tian, Z., and Wang, T.: Considerable Model–Data Mismatch in
713 Temperature over China during the Mid-Holocene: Results of PMIP Simulations, Journal
714 of Climate, 25, 4135-4153, 2012.

715 Jiang, D., Tian, Z., and Lang, X.: Mid-Holocene net precipitation changes over China:
716 model-data comparison, Quaternary Science Reviews, 82, 104-120, 2013.

717 Jiang, D., Tian, Z., and Lang, X.: Reliability of climate models for China through the IPCC
718 Third to Fifth Assessment Reports, International Journal of Climatology, 36, 1114-1133,
719 2016.

720 Jiang, Q., and Piperno., R. D.: Environmental and archaeological implications of a late
721 Quaternary palynological sequence, Poyang lake, Southern China, Quaternary Research,
722 52, 250-258, 1999.

723 Jiang, W., Guiot, J., Chu, G., Wu, H., Yuan, B., Hatté, C., and Guo, Z.: An improved
724 methodology of the modern analogues technique for palaeoclimate reconstruction in arid
725 and semi-arid regions, Boreas, 39, 145-153, 2010.

726 Jiang, W., Guo, Z., Sun, X., Wu, H., Chu, G., Yuan, B., Hatte, C., and Guiot, J.:
727 Reconstruction of climate and vegetation changes of Lake Bayanchagan (Inner Mongolia):
728 Holocene variability of the East Asian monsoon. Quaternary Research, 65, 411-420, 2006.

729 Jiang, W., Leroy, S. G., Ogle, N., Chu, G., Wang, L., and Liu, J.: Natural and authropogenic
730 forest fires recorded in the Holocene pollen record from a Jinchuan peat bog, northeastern
731 China, Palaeogeography, Palaeoclimatology, Palaeoecology, 261, 47-57, 2008.

732 Joussaume, S., and Taylor, K. E.: Status of the Paleoclimate Modeling Intercomparison Project,
733 Proceedings of the First International AMIP Scientific Conference, 425-430, 1995.

734 Joussaume, S., Taylor, K. E., Braconnot, P., Mitchell, J. F. B., Kutzbach, J. E., Harrison, S. P.,
735 Prentice, I. C., Broccoli, A. J., Abe-Ouchi, A., Bartlein, P. J., Bonfils, C., Dong, B., Guiot,
736 J., Herterich, K., Hewitt, C. D., Jolly, D., Kim, J. W., Kislov, A., Kitoh, A., Loutre, M. F.,
737 Masson, V., McAvaney, B., McFarlane, N., de Noblet, N., Peltier, W. R., Peterschmitt, J. Y.,
738 Pollard, D., Rind, D., Royer, J. F., Schlesinger, M. E., Syktus, J., Thompson, S., Valdes, P.,
739 Vettoretti, G., Webb, R. S., Wyputta, U.: Monsoon changes for 6000 years ago: Results of

740 18 simulations from the Paleoclimate Modeling Intercomparison Project (PMIP),
741 Geophysical Research Letters, 26, 856-862, 1999.

742 Kaplan, J. O., Bigelow, N. H., Bartlein, P. J., Christensen, T. R., Cramer, W., Harrison, S. P.,
743 Matveyeva, N. V., McGuire, A. D., Murray, D. F., Prentice, I. C., Razzhivin, V. Y., Smith,
744 B., Anderson, P. M., Andreev, A. A., Brubaker, L. B., Edwards, M. E., and Lozhkin, A. V.:
745 Climate change and Arctic ecosystems: 2. Modeling, palaeodata-model comparisons, and
746 future projections, Journal of Geophysical Research: Atmospheres, 108, 8171,
747 doi:10.1029/2002JD002559, 2003.

748 Kohfeld, K. E. and Harrison, S.: How well we can simulate past climates? Evaluating the
749 models using global palaeoenvironmental datasets, Quaternary Science Reviews, 19,
750 321-346, 2000.

751 Kong, Z., Xu, Q., Yang, X., Sun, L., Liang, W.: Analysis of sporopollen assemblages of
752 Holocene alluvial deposits in the Yinmahe River Basin, Hebei Province, and preliminary
753 study on temporal and spatial changes of vegetation, Acta Phytoecologica Sinica, 24, 724,
754 2000 (in Chinese with English abstract).

755 Lee, Y., and Liew, M.: Pollen stratigraphy, vegetation and environment of the last glacial and
756 Holocene-A record from Toushe Basin, central Taiwan,
757 Palaeogeography, Palaeoclimatology, Palaeoecology, 287, 58-66, 2010.

758 Li, B., and Sun, J.: Vegetation and climate environment during Holocene in Xi'an region of
759 Loess Plateau, China, Marine Geology and Quaternary Geology, 3, 125-132, 2005 (in
760 Chinese with English abstract).

761 Li, C., Wu, Y., and Hou, X.: Holocene vegetation and climate in Northeast China revealed
762 from Jingbo Lake sediment, Quaternary International, 229, 67-73, 2011.

763 Li, L., Lin, P., Yu, Y., Wang, B., Zhou, T., Liu, L., Liu, J., Bao, Q., Xu, S., Huang, W., Xia,
764 K., Pu, Y., Dong, L., Shen, S., Liu, Y., Hu, N., Liu, M., Sun, W., Shi, X., Zheng, W., Wu,
765 B., Song, M., Liu, H., Zhang, X., Wu, G., Xue, W., Huang, X., Yang, G., Song, Z., and
766 Qiao, F.: The flexible global ocean-atmosphere-land system model, Grid-point Version 2:
767 FGOALS-g2, Advances in Atmospheric Sciences, 30, 543-560, 2013.

768 Li, Q., Wu, H., Guo, Z., Yu, Y., Ge, J., Wu, J., Zhao, D., and Sun, A.: Distribution and
769 vegetation reconstruction of the deserts of northern China during the mid-Holocene,
770 Geophysical Research Letter, 41, 2184-5191, 2014.

771 Li, X., and Liu, J.: Holocene vegetational and environmental changes at Mt. Luoji, Sichuan,
772 Acta Geographica Sinica, 1, 44-51, 1988 (in Chinese with English abstract).

773 Li, X., Zhao, K., Dodson, J., and Zhou, X.: Moisture dynamics in central Asia for the last
774 15 kyr: new evidence from Yili Valley, Xinjiang, NW China, Quaternary Science
775 Reviews, 30, 23-34, 2011.

776 Li, X., Zhou, J., and Dodson, J.: The vegetation characteristics of the ‘yuan’ area at Yaoxian
777 on the loess plateau in china over the last 12 000 years. Review of Palaeobotany &
778 Palynology, 124, 1-7, 2003.

779 Li, X., Zhou, W., An, Z., and Dodson, J.: The vegetation and monsoon variations at the
780 desert-loess transition belt at Midiwan in northern China for the last 13 ka, Holocene, 13,
781 779-784, 2003.

782 Li, Z., Hai, Y., Zhou, Y., Luo, R., Zhang, Q.: Pollen Component of Lacustrain Deposit and its
783 Palaeo-environment Significance in the Downstream Region of Urumqi Riever since
784 30Ka BP, Arid Land Geography, 24, 201-205, 2001 (in Chinese with English abstract).

785 Liu, H., Cui, H., Tian, Y., and Xu, L.: Temporal-spatial variances of Holocene precipitation at
786 the Marginal area of the East Monsoon influences from pollen evidence, Acta Botanica
787 Sinica, 44, 864-871, 2002 (in Chinese with English abstract).

788 Liu, H., Tang, X., Sun, D., and Wang, K.: Palynofloras of the Dajiuhu Basin in Shennongjia
789 mountains during the last 12.5 ka, Acta Micropalaeontologica Sinica, 1, 101-109, 2001 (in
790 Chinese with English abstract).

791 Liu, J., Zhao, S., Cheng, J., Bao, J., and Yin, G.: A study of vegetation and climate evolution
792 since the Holocene near the banks of the Qiangtang River in Hangzhou Bay, Earth
793 Science Frontiers, 5, 235-245, 2007 (in Chinese with English abstract).

794 Liu, M., Huang, Y., and Kuo, M.: Pollen stratigraphy, vegetation and environment of the last
795 glacial and Holocene-A record from Toushe Basin, central Taiwan, Quaternary
796 International, 14, 16-33, 2006.

797 Liu, Y., Liu, J., and Han, J.: Pollen record and climate changing since 12.0ka B. P. in
798 Erlongwan Maar Lake, Jilin province, Journal of Jilin University (Earth Science Edition),
799 39, 93-98, 2009 (in Chinese with English abstract).

800 Liu, Y., Zhang, S., Liu, J., You, H., and Han, J.: Vegetation and environment history of
801 erlongwan Maar lake during the late Pleistocene on pollen record, Acta
802 Micropalaeontologica Sinica, 25, 274-280, 2008 (in Chinese with English abstract).

803 Liu, Z., Harrison, S. P., Kutzbach, J. E., and Otto-Bliesner, B.: Global monsoons in the
804 mid-Holocene and oceanic feedback, Climate Dynamics, 22, 157-182, 2004.

805 Liu, Z., Wang, Y., Gallimore, R., Gasse, F., Johnson, T., deMenocal, P., Adkins, J., Notaro, M.,
806 Prentice, I.C., Kutzbach, J., Jacob, R., Behling, P., Wang, L., and Ong, E.: Simulating the

807 transient evolution and abrupt change of Northern Africa atmosphere–ocean–terrestrial
808 ecosystem in the Holocene, Quaternary Science Reviews, 26, 1818-1837, 2007.

809 Liu, Z., Zhu, J., Rosenthal, Y., Zhang, X., Otto-Bliesner, B. L., Timmermann, A., Smith, R. S.,
810 Lohmann, G., Zheng, W., and Elison Timm, O.: The Holocene temperature conundrum,
811 Proceedings of the National Academy of Sciences, 111, E3501-E3505, 2014.

812 Lu, H., Wu, N., Liu, K.-b., Zhu, L., Yang, X., Yao, T., Wang, L., Li, Q., Liu, X., Shen, C., Li, X.,
813 Tong, G., and Jiang, H.: Modern pollen distributions in Qinghai-Tibetan Plateau and the
814 development of transfer functions for reconstructing Holocene environmental changes,
815 Quaternary Science Reviews, 30, 947-966, 2012.

816 Luo, H.: Characteristics of the Holocene sporopollen flora and climate change in the Coqên
817 area, Tibet, Chengdu University of Technology, Master Dissertation, 2008 (in Chinese
818 with English abstract).

819 Mann, M. E., Zhang, Z., Hughes, M. K., Bradley, R. S., Miller, S. K., Rutherford, S., and Ni, F.:
820 Proxy-based reconstructions of hemispheric and global surface temperature variations over
821 the past two millennia, Proceedings of the National Academy of Sciences, 105,
822 13252-13256, 2008.

823 Marchant, R., Cleef, A., Harrison, S. P., Hooghiemstra, H., Markgraf, V., Van Boxel, J., Ager,
824 T., Almeida, L., Anderson, R., Baied, C., Behling, H., Berrio, J. C., Burbridge, R., Bjorck,
825 S., Byrne, R., Bush, M., Duivenvoorden, J., Flenley, J., De Oliveira, P., Van Gee, B., Graf,
826 K., Gosling, W. D., Harbele, S., Van Der Hammen, T., Hansen, B., Horn, S., Kuhry, P.,
827 Ledru, M. P., Mayle, F., Leyden, B., Lozano-Garcia, S., Melief, A. M., Moreno, P., Moar,
828 N. T., Prieto, A., Van Reenen, G., Salgado-Labouriau, M., Schabitz, F., Schreve-Brinkman,
829 E. J., and Wille, M.: Pollen-based biome reconstructions for Latin America at 0, 6000 and
830 18 000 radiocarbon years ago, Climate of the Past, 5, 725-767, 2009.

831 Marcott, S., Shakun, J., U Clark, P., and Mix, A.: A Reconstruction of Regional and Global
832 Temperature for the Past 11,300 Years, Science, 1198-1201, 2013.

833 Mauri, A., Davis, B. A. S., Collins, P. M., and Kaplan, J. O.: The climate of Europe during the
834 Holocene: a gridded pollen-based reconstruction and its multi-proxy evaluation,
835 Quaternary Science Reviews, 112, 109-127, 2015.

836 Ma, Y., Zhang, H., Pachur, H., Wunnemann, B., Li, J., and Feng, Z.: Late Glacial and
837 Holocene vegetation history and paleoclimate of the Tengger Desert, northwestern China,
838 Chinese Science Bulletin, 48, 1457-1463, 2003.

839 Members of the China Quaternary Pollen Data Base.: Pollen-based Biome reconstruction at
840 Middle Holocene (6 ka BP) and Last Glacial Maximum (18 ka BP) in China, Acta Botanica
841 Sinica, 42, 1201-1209, 2000 (in Chinese with English abstract).

842 Members, M. P.: Constraints on the magnitude and patterns of ocean cooling at the Last Glacial
843 Maximum, Nature Geoscience, 2, 127-130, 2009.

844 Meng, X., Zhu, D., Shao, Z., Han, J., Yu, J., Meng, Q., Lv, R., and Luo, P.: Paleoclimatic and
845 Plaeoenvironmental Evolution Since Holocene in the Ningwu Area, Shanxi Province, Acta
846 Geologica Sinica, 3, 316-323, 2007 (in Chinese with English abstract).

847 Ni, J., Sykes, M. T., Prentice, I. C., and Cramer, W.: Modelling the vegetation of China using
848 the process-based equilibrium terrestrial biosphere model BIOME3, Global Ecology and
849 Biogeography, 9, 463-479, 2000.

850 Ni, J., Yu, G., Harrison, S.P., Prentice, I. C.: Palaeovegetation in China during the late
851 Quaternary: Biome reconstructions based on a global scheme of plant functional types,
852 Palaeogeography, Palaeoclimatology, Palaeoecology, 289, 44-61, 2010.

853 Oguntunde, P. G., Ajayi, A. E., and Giesen, N.: Tillage and surface moisture effects on
854 bare-soil albedo of a tropical loamy sand, Soil and Tillage Research, 85, 107-114, 2006.

855 O'ishi, R., A. Abe‐Ouchi, I. C. Prentice, and S. Sitch.: Vegetation dynamics and plant CO_2
856 responses as positive feedbacks in a greenhouse world, Geophysical Research Letters, 36,
857 L11706, doi: 10.1029/2009GL038217, 2009.

858 Otto, J., T. Raddatz, M. Claussen, V. Brovkin, and V. Gayler.: Separation of
859 atmosphere-ocean-vegetation feedbacks and synergies for mid-Holocene climate,
860 Geophysical Research Letters, 36, L09701, doi: 10.1029/2009GL037482, 2009.

861 Peyron, O., Guiot, J., Cheddadi, R., Tarasov, P., Reille, M., De Beaulieu, J.L., Bottema, S., and
862 Andrieu, Valerie. : Climatic reconstruction in Europe for 18,000 YR B.P. from pollen data,
863 Quaternary Research, 49, 183-196, 1998.

864 Peyron, O., Jolly, D., Bonnefille, R., Vincens, A., and Guiot, J.: Climate of East Africa 6000
865 ^{14}C yr B.P. as Inferred from Pollen Data, Quaternary Research, 54, 90-101, 2000.

866 Pickett Elizabeth, J., Harrison Sandy, P., Hope, G., Harle, K., Dodson John, R., Peter Kershaw,
867 A., Colin Prentice, I., Backhouse, J., Colhoun Eric, A., D'Costa, D., Flenley, J., Grindrod, J.,
868 Haberle, S., Hassell, C., Kenyon, C., Macphail, M., Martin, H., Martin Anthony, H.,
869 McKenzie, M., Newsome Jane, C., Penny, D., Powell, J., Ian Raine, J., Southern, W.,
870 Stevenson, J., Sutra, J. P., Thomas, I., Kaars, S., and Ward, J.: Pollen-based reconstructions
871 of biome distributions for Australia, Southeast Asia and the Pacific (SEAPAC region) at 0,
872 6000 and 18,000 ^{14}C yr BP, Journal of Biogeography, 31, 1381-1444, 2004.

873 Prentice, I. C., Guiot, J., Huntley, B., Jolly, D., and Cheddadi, R.: Reconstructing biomes from
874 palaeoecological data: A general method and its application to European pollen data at 0
875 and 6 ka, Climate Dynamics, 12, 185-194, 1996.

876 Prentice, I. C., and Jolly, D.: Mid-Holocene and glacial-maximum vegetation geography of the
877 northern continents and Africa, Journal of Biogeography, 27, 507-519, 2000.

878 Reimer, P. J., Bard, E., Bayliss, A., Beck, J. W., Blackwell, P. G., Ramsey, C. B., Buck, C. E.,
879 Cheng, H., Edwards, R. L., Friedrich, M., Grootes, P. M., Guilderson, T. P., Haflidason, H.,
880 Hajdas, I., Hatté, C., Heaton, T. J., Hoffmann, D. L., Hogg, A. G., Hughen, K. A., Kaiser, K.
881 F., Kromer, B., Manning, S. W., Niu, M., Reimer, R. W., Richards, D. A., Scott, E. M.,
882 Southon, J. R., Staff, R. A., Turney, C. S. M. and van der Plicht, J.: IntCal13 and Marine13
883 Radiocarbon Age Calibration Curves 0–50,000 Years cal BP, Radiocarbon, 55(4),
884 1869–1887, doi:DOI: 10.2458/azu_js_rc.55.16947, 2013.

885 Schmidt, G.A., Annan, J.D., Bartlein, P.J., Cook, B.I., Guilyardi, E., Hargreaves, J.C.,
886 Harrison, S.P., Kageyama, M., Legrande, A.N., Konecky, B.L., Lovejoy, S., Mann, M.E.,
887 Masson-Delmotte, V., Risi, C., Thompson, D., Timmermann, A., and Yiou, P.: Using
888 palaeo-climate comparisons to constrain future projections in CMIP5, Climate of the Past,
889 10, 221-250, 2014a.

890 Schmidt, G.A., Kelley, M., Nazarenko, L., Ruedy, R., Russell, G.L., Aleinov, I., Bauer, M.,
891 Bauer, S.E., Bhat, M.K., Bleck, R., Canuto, V., Chen, Y., Cheng, Y., Clune, T.L., Del
892 Genio, A., de Fainchtein, R., Faluvegi, G., Hansen, J.E., Healy, R.J., Kiang, N.Y., Koch,
893 D., Lacis, A.A., Legrande, A.N., Lerner, J., Lo, K.K., Matthews, E.E., Menon, S., Miller,
894 R.L., Oinas, V., Oloso, A.O., Perlwitz, J.P., Puma, M.J., Putman, W.M., Rind, D.,
895 Romanou, A., Sato, M., Shindell, D.T., Sun, S., Syed Rahman, A., Tausnev, N., Tsigaridis,
896 K., Under, N., Voulgarakis, A., Yao, M., and Zhang, J.: Configuration and assessment of
897 the GISS ModelE2 contributions to the CMIP5 archive, Journal of Advances in Modeling
898 Earth Systems, 6, 141-184, 2014b.

Shakun, J. D., Clark, P. U., He, F., Marcott, S. A., Mix, A. C., Liu, Z., Otto-Bliesner, B., Schmittner, A., and Bard, E.: Global warming preceded by increasing carbon dioxide concentrations during the last deglaciation, Nature, 484, 49-55, 2012.

Shen, C., Liu, K., Tang, L., Overpeck, J. T.: Quantitative relationships between modern pollen rain and climate in the Tibetan Plateau, Review of Palaeobotany and Palynology, 140, 61-77, 2006.

Shen, J., Jones, R. T., Yang, X., Dearing, J. A., and Wang, S.: The Holocene vegetation history of lake Erhai, Yunnan province southwestern china: the role of climate and human forcings, The Holocene, 16, 265-276, 2006.

Shen, J., Liu, X., Matsumoto, R., Wang, S., Yang, X., Tang, L., and Shen, C.: Multi-index high-resolution paleoclimatic evolution of sediments in Qinghai Lake since the late glacial period, Science in China Series D: Earth Sciences, 6, 582-589, 2004 (in Chinese with English abstract).

Shu, J., Wang, W., and Chen, Y.: Holocene vegetation and environment changes in the NW Taihu Plain, Jiangsu Province, East China, Acta Micropalaeontologica Sinica, 2, 210-221, 2007 (in Chinese with English abstract).

Shu, Q., Xiao, J., Zhang, M., Zhao, Z., Chen, Y., and Li, J.: Climate Change in Northern Jiangsu Basin since the Last Interglacial: Geological Science and Technology Information, 5, 59-64, 2008 (in Chinese with English abstract).

Song, M., Zhou, C., and Ouyang, H.: Simulated distribution of vegetation types in response to climate change on the Tibetan Plateau, Journal of Vegetation Science, 16, 341-350, 2005.

Sun, A., and Feng, Z.: Holocene climate reconstructions from the fossil pollen record at Qigai Nuur in the southern Mongolian Plateau, The Holocene, 23, 1391-1402, 2013.

Sun, L., Xu, Q., Yang, X., Liang, W., Sun, Z., and Chen, S.: Vegetation and environmental changes in the Xuanhua Basin of Hebei Province since Postglacial, Journal of Geomechanics, 4, 303-308, 2001 (in Chinese with English abstract).

Sun, Q., Zhou, J., Shen, J., Cheng, P., Wu, F., and Xie, X.: Mid-Holocene environmental characteristics recorded in the sediments of the Bohai Sea in the northern environmental sensitive zone, Science in China Series D: Earth Sciences, 9, 838-849, 2006 (in Chinese with English abstract).

Sun, X., and Xia, Z.: Paleoenvironment Changes Since Mid-Holocene Revealed by a Palynological Sequence from Sihenan Profile in Luoyang, Henan Province, Acta Scientiarum Naturalium Universitatis Pekinensis, 2, 289-294, 2005 (in Chinese with English abstract).

Sun. X., Wang. F., and Sun. C.: Pollen-climate response surfaces of selected taxa from Northern China, Science in China Series D: Earth Sciences, 39, 486, 1996.

Swann, A. L., Fung, I. Y., Levis, S., Bonan, G. B., and Doney, S. C.: Changes in Arctic vegetation amplify high-latitude warming through the greenhouse effect, Proceedings of the National Academy of Sciences, 107, 1295-1300, 2010.

Sykes, M.T., Prentice, I.C., and Laarif, F.: Quantifying the impact of global climate change on potential natural vegetation, Climatic Change, 41, 37–52, 1999.

Tang, L., and An, C.: Holocene vegetation change and pollen record of drought events in the Loess Plateau, Progress in Natural Science, 10,1371-1382, 2007 (in Chinese with English abstract).

Tang, L., and Shen, C.: Holocene pollen records of the Qinghai-Xizang Plateau, Acta Micropalaeontologica Sinica, 4, 407-422, 1996 (in Chinese with English abstract).

945 Tang, L., Shen, C., Kong, Z., Wang, F., and Liao, K.: Pollen evidence of climate during the
946 last glacial maximum in Eastern Tibetan Plateau, Journal of Glaciology, 2, 37-44, 1998
947 (in Chinese with English abstract).

948 Tang, L., Shen, C., Li, C., Peng, J., and Liu, H.: Pollen-inferred vegetation and environmental
949 changes in the central Tibetan Plateau since 8200 yr B.P., Science in China Series D:
950 Earth Sciences, 5, 615-625, 2009 (in Chinese with English abstract).

951 Tao, S., An, C., Chen, F., Tang, L., Wang, Z., Lv, Y., Li, Z., Zheng, T., and Zhao, J.:
952 Vegetation and environment since the 16.7cal ka B.P. in Balikun Lake, Xinjiang, China,
953 Chinese Science Bulletin, 11, 1026-1035, 2010 (in Chinese with English abstract).

954 Taylor, K.E., Crucifix, M., Braconnot, P., Hewitt, C. D., Doutriaux. C., Broccoli, A. J., Mitchell,
955 J. F. B., Webb, M. J.: Estimating shortwave radiative forcing and response in climate
956 models, Journal of Climate, 20, 2530-2543, 2007.

957 Taylor, K.E., Stouffer, R.J., Meehl, G.A.: An overview of CMIP5 and the experiment design,
958 Bulletin of the American Meteorological Society, 93, 485-498, 2012.

959 Voldoire, A., Sanchez-Gomez, E., Salas y Melia, D., Decharme, B., Cassou, C.,Senesi, S.,
960 Valcke, S., Beau, I., Alias, A., Chevallier, M., Deque, M., Deshayes, J., Douville, H.,
961 Fernandez, E., Madec, G., Maisonnave, E., Moine, M., Planton, S., Saint-Martin, D.,
962 Szopa, S., Tyteca, S., Alkama, R., Belamari, S., Braun, A., Coquart, L., and Chauvin, F.:
963 The CNRM-CM5.1 global climate model: description and basic evaluation, Climate
964 Dynamics, 40, 2091-2121, 2012.

965 Wang, H., Liu, H., Zhu, J., and Yin, Y.: Holocene environmental changes as recorded by
966 mineral magnetism of sediments from Anguli-nuur Lake, southeastern Inner Mongolia
967 Plateau, China, Palaeogeography, Palaeoclimatology, Palaeoecology, 285, 30-49, 2010.

968 Wang, S., Lv, H., and Liu, J.: Environmental characteristics of the early Holocene suitable
969 period revealed by the high-resolution sporopollen record of Huguangyan Lake, Chinese
970 Science Bulletin, 11, 1285-1291, 2007 (in Chinese with English abstract).

971 Wang, X., Wang, J., Cao, L., Yang, J., Yang, X., Peng, Z., and Jin, G.: Late Quaternary
972 Pollen Records and Climate Significance in Guangzhou, Acta Scientiarum Naturalium
973 Universitatis Sunyatseni, 3, 113-121, 2010 (in Chinese with English abstract).

974 Wang, X., Zhang, G., Li, W., Zhang, X., Zhang, E., and Xiao, X.: Environmental changes
975 during early-middle Holocene from the sediment record of the Chaohu Lake, Anhui
976 Province, Chinese Science Bulletin, 53, 153-160, 2008.

977 Wang, Y., Wang, S., Jiang, F., and Tong, G.: Palynological records in Xipu section,
978 Yangyuan, Journal of Geomechanics, 2, 171-175, 2003 (in Chinese with English abstract).

979 Wang, Y., Wang, S., Zhao, Z., Qin, Y., Ma, Y., Sun, J., Sun, H., and Tian, M.: Vegetation and
980 Environmental Changes in Hexiqten Qi of Inner Mongolia in the Past 16000 Years, Acta
981 Geoscientica Sinica, 5, 449-453, 2005 (in Chinese with English abstract).

982 Wang, Y., Zhao, Z., Qiao, Y., Wang, S., Li, C., and Song, L.: Paleoclimatic and
983 paleoenvironmental evolution since the late glacial epoch as recorded by sporopollen from
984 the Hongyuan peat section on the Zoigê Plateau, northern Sichuan, China, Geological
985 Bulletin of China, 7, 827-832, 2006 (in Chinese with English abstract).

986 Watanabe, S., Hajima, T., Sudo, K., Nagashima, T., Takemura, T., Okajima, H., Nozawa, T.,
987 Kawase, H., Abe, M., Yokohata, T., Ise, T., Sato, H., Kato, E., Takata, K., Emori, S., and
988 Kawamiya, M.: MIROC-ESM 2010: model description and basic results of
989 CMIP5-20c3m experiments, Geoscientific Model Development, 4, 845-872, 2011.

990 Webb, III. T.: Global paleoclimatic data base for 6000 yr BP, Brown Univ., Providence, RI
991 (USA). Dept. of Geological Sciences, DOE/EV/10097-6; Other: ON: DE85006628 United
992 States Other: ON: DE85006628 NTIS, PC A08/MF A01. HEDB English, 1985.

993 Wen, R., Xiao, J., Chang, Z., Zhai, D., Xu, Q., Li, Y. and Itoh, S.: Holocene precipitation and
994 temperature variations in the East Asian monsoonal margin from pollen data from Hulun
995 Lake in northeastern Inner Mongolia, China, Boreas, 39, 262-272, 2010.

996 Weninger, B., Jöris, O., Danzeglocke, U.: CalPal-2007, Cologne Radiocarbon Calibration and
997 Palaeoclimate Research Package, http://www.calpal.de/, 2007.

998 Wischnewski, J., Mischke, S., Wang, Y., and Herzschuh, U.: Reconstructing climate
999 variability on the northeastern Tibetan Plateau since the last Lateglacial – a multi-proxy,
1000 dual-site approach comparing terrestrial and aquatic signals, Quaternary Science Reviews,
1001 30, 82-97, 2011.

1002 Wohlfahrt, J., Harrison, S. P., and Braconnot, P.: Synergistic feedbacks between ocean and
1003 vegetation on mid- and high-latitude climates during the mid-Holocene, Climate Dynamics,
1004 22, 223-238, 2004.

1005 Wu, H., Guiot, J., Brewer, S., and Guo, Z.: Climatic changes in Eurasia and Africa at the last
1006 glacial maximum and mid-Holocene: reconstruction from pollen data using inverse
1007 vegetation modeling, Climate Dynamics, 29, 211-229, 2007.

1008 Wu, H., Luo, Y., Jiang, W., Li, Q., Sun, A., and Guo, Z.: Paleoclimate reconstruction from
1009 pollen data using inverse vegetation approach: Validation of model using modern data,
1010 Quaternary Sciences, 36, 520-529, 2016 (in Chinese with English abstract).

1011 Wu, H., Ma, Y., Feng, Z., Sun, A., Zhang, C., Li, F., and Kuang, J.: A high resolution record
1012 of vegetation and environmental variation through the last ~25,000 years in the western

1013 part of the Chinese Loess Plateau, Palaeogeography, Palaeoclimatology, Palaeoecology,
1014 273, 191-199, 2009.

1015 Xia, Y.: Preliminary study on vegetational development and climatic changes in the Sanjiang
1016 Plain in the last 12000 years, Scientia Geographica Sinica, 8, 241-249, 1988 (in Chinese
1017 with English abstract).

1018 Xia, Z., Chen, G., Zheng, G., Chen, F., and Han, J.: Climate background of the evolution from
1019 Paleolithic to Neolithic cultural transition during the last deglaciation in the middle
1020 reaches of the Yellow River, Chinese Science Bulletin, 47, 71-75, 2002.

1021 Xiao, J., Lv, H., Zhou, W., Zhao, Z., and Hao, R.: Pollen Vegetation and Environmental
1022 Evolution of the Great Lakes in Jiangxi Province since the Last Glacial Maximum,
1023 Science in China Series D: Earth Sciences, 6, 789-797, 2007 (in Chinese with English
1024 abstract).

1025 Xiao, J., Xu, Q., Nakamura, T., Yang, X., Liang, W., and Inouchi, Y.: Holocene vegetation
1026 variation in the Daihai Lake region of north-central China: a direct indication of the Asian
1027 monsoon climatic history, Quaternary Science Reviews, 23, 1669-1679, 2004.

1028 Xiao, X., Haberle, S. G., Shen, J., Yang, X., Han, Y., Zhang, E., and Wang, S.: Latest
1029 Pleistocene and Holocene vegetation and climate history inferred from an alpine
1030 lacustrine record, northwestern Yunnan Province, southwestern China, Quaternary
1031 Science reviews, 86, 35-48, 2014.

1032 Xie, Y., Li, C., Wang, Q., and Yin, H.: Climatic Change since 9 ka B. P.: Evidence from
1033 Jiangling Area, Jianghan Plain, China, Scientia Geographica Sinica, 2, 199-204, 2006 (in
1034 Chinese with English abstract).

1035 Xin, X., Wu, T., and Zhang, J.: Introduction of CMIP5 experiments carried out with the
1036 climate system models of Beijing climate Center, Advances in Climate Change Research,
1037 4, 41-49, 2013.

1038 Xu, J.: Analysis of the Holocene Loess Pollen in Xifeng Area and its Vegetation Evolution,
1039 Capital Normal University, Master Dissertation, 2006 (in Chinese with English abstract).

1040 Xu, Q., Chen, S., Kong, Z., and Du, N.: Preliminary discussion of vegetation succession and
1041 climate change since the Holocene in the Baiyangdian Lake district, Acta Phytoecologica
1042 and Geobotanica Sinica, 2, 65-73, 1988 (in Chinese with English abstract).

1043 Xu, Q., Yang, Z., Cui, Z., Yang, X., and Liang.: A Study on Pollen Analysis of Qiguoshan
1044 Section and Ancestor Living Environment in Chifeng Area, Nei Mongol, Scientia
1045 Geographica Sinica, 4, 453-456, 2002 (in Chinese with English abstract).

1046 Xu, Y.: The assemblage of Holocene spore pollen and its environment in Bosten Lake area
1047 Xinjiang, Arid land Geography, 2, 43-49, 1998 (in Chinese with English abstract).

1048 Xue, S., and Li, X.: Holocene vegetation characteristics of the southern Loess Plateau in the
1049 Weihe River valley in China, Review of Palaeobotany & Palynology, 160 46-52, 2010.

1050 Yang, J., Cui, Z., Yi, Zhao., Zhang, W., and Liu, K.: Glacial Lacustrine Sediment's Response
1051 to Climate Change since Holocene in Diancang Mountain, Acta Geographica Sinica, 4,
1052 525-533, 2004 (in Chinese with English abstract).

1053 Yang, X., Wang, S., and Tong, G.: Character of anology and changes of monsoon climate
1054 over the last 10000 years in Gucheng Lake, Jiangsu province, Journal of Integrative Plant
1055 Biology, 7, 576-581, 1996 (in Chinese with English abstract).

1056 Yang, Y., and Wang, S.: Study on mire development and paleoenvironment change since
1057 8.0ka B.P. in the northern part of the Sangjiang Plain, Scientia Geographica Sinica, 23,
1058 32-38, 2003 (in Chinese with English abstract).

1059 Yang, Z.: Reconstruction of climate and environment since the Holocene in Diaojiaohaizi
1060 Lake Area, Daqing Mountains,Inner Mongolia, Acta Ecologica Sinica, 4, 538-543, 2001
1061 (in Chinese with English abstract).

1062 Yu, L., Wang, N., Cheng, H., Long, H., and Zhao, Q.: Holocene environmental change in the
1063 marginal area of the Asian monsoon: a record from Zhuye Lake, NW china, Boreas, 38,
1064 349-361, 2009.

1065 Yukimoto, S., Adachi, Y., Hosaka, M., Sakami, T., Yoshimura, H., Hirabara, M., Tanaka,
1066 T.Y., Shindo, E., Tsujino, H., Deushi, M., Mizuta, R., Yabu, S., Obata, A., Nakano, H.,
1067 Koshiro, T., Ose, T., and Kitoh, A.: A new global climate model of the meteorological
1068 research institute: MRI-CGCM3-model description and basic performance, Journal of the
1069 Meterological Society of Japan, 90A, 23-64, 2012.

1070 Zhang, W., Mu, K., Cui, Z., Feng, J., and Yang, J.: Record of the environmental change since
1071 Holocene in the region of Gongwang mountain, Yunan Province, Earth and Environment,
1072 4, 343-350, 2007 (in Chinese with English abstract).

1073 Zhang, Y. G., Pagani, M., and Liu, Z.: A 12-Million-Year Temperature History of the tropical
1074 Pacific Ocean, Science, 344, 84-87, 2014.

1075 Zhang, Y., and Yu, S.: Palynological assemblages of late Quaternary from the Shenzhen
1076 region and its paleoenvironment evolution, Marine Geology & Quaternary Geology, 2,
1077 109-114, 1999 (in Chinese with English abstract).

1078 Zhang, Y., Jia, L., and Lyu, B.: Studies on Evolution of Vegetation and Climate since 7000
1079 Years ago in Estuary of Changjiang River Region, Marine Science Bulletin, 3, 27-34,
1080 2004 (in Chinese with English abstract).

1081 Zhang, Y., Song, M., and Welker, J. M.: Simulating Alpine Tundra Vegetation Dynamics in
1082 Response to Global Warming in China, Global Warming, Stuart Arthur Harris (Ed.),
1083 ISBN: 978-953-307-149-7, InTech, 11, 221-250, 2010.

1084 Zhang, Z., Xu, Q., Li, Y., Yang, X., Jin, Z., and Tang, J.: Environmental changes of the Yin
1085 ruins area based on pollen analysis, Quaternary Science, 27, 461-468, 2007 (in Chinese
1086 with English abstract).

1087 Zhao, J., Hou, Y., Du, J., and Chen, Y.: Holocene environmental changes in the Guanzhong
1088 Plain, Arid Land Geography, 1, 17-22, 2003 (in Chinese with English abstract).

1089 Zhao, Y., Yu, Z., Chen, F., Ito, E., and Zhao, C.: Holocene vegetation and climate history at
1090 Hurleg Lake in the Qaidam Basin, northwest China, Review of Palaeobotany and
1091 palynology, 145, 275-288, 2007.

1092 Zheng, R., Xu, X., Zhu, J., Ji, F., Huang, Z., Li, J.: Division of late Quaternary strata and
1093 analysis of palaeoenvironment in Fuzhou Basin, Seismology and Geology, 4, 503-513,
1094 2002 (in Chinese with English abstract).

1095 Zheng, X., Zhang, H., Ming, Q., Chang, F., Meng, H., Zhang, W., Liu, M., Shen, C.:
1096 Vegetational and environmental changes since 15ka B.P. recorded by lake Lugu in the
1097 southwest monsoon domain region, Quaternary Sciences, 6, 1314-1326, 2014 (in Chinese
1098 with English abstract).

1099 Zhou, J., Liu, D., Zhuang, Z., Wang, Z., and Liu, L.: The sediment layers and the records of
1100 the Paleoenvironment in the Chaoyanggang Lagoon,Rongcheng City of Shandong

Province Since Holocene Transgression, Periodical of Ocean University of China, 38, 803-808, 2008 (in Chinese with English abstract).

Zhu, C., Ma, C., Zhang, W., Zheng, C., Tan, L., Lu, X., Liu, K., and Chen, H.: Pollenrecord from Dajiuhu Basin of Shennongjia and environmental changes since 15.753 ka B.P., Quaternary Sciences, 5, 814-826, 2006 (in Chinese with English abstract).

Zou, S., Cheng, G., Xiao, H., Xu, B., and Feng, Z.: Holocene natural rhythms of vegetation and present potential ecology in the western Chinese Loess Plateau, Quaternary International, 194, 55-67, 2009.

1122 **Table 1. Basic information of the pollen dataset used in this study**

Site	Lat	Lon	Alt	Webb 1-7	Source
Sujiawan	35.54	104.52	1700	2	original data (Zou et al., 2009)
Xiaogou	36.10	104.90	1750	2	original data (Wu et al., 2009)
Dadiwan	35.01	105.91	1400	1	original data (Zou et al., 2009)
Sanjiaocheng	39.01	103.34	1320	1	Chen et al., 2006
Chadianpo	36.10	114.40	65	2	Zhang et al., 2007
Qindeli	48.08	133.25	60	2	Yang and Wang, 2003
Fuyuanchuangye	47.35	133.03	56	3	Xia, 1988
Jingbo Lake	43.83	128.50	350	2	Li et al., 2011
Hani Lake	42.22	126.52	900	1	Cui et al., 2006
Jinchuan	42.37	126.43	662	5	Jiang et al., 2008
Maar Lake	42.30	126.37	724	1	Liu et al., 2009
Maar Lake	42.30	126.37	724	1	Liu et al., 2008
Xie Lake SO4	37.38	122.52	0	1	Zhou et al., 2008
Nanhuiheming Core	31.05	121.58	7	2	Jia and Zhang, 2006
Toushe	23.82	120.88	650	1	Liu et al., 2006
Dongyuan Lake	22.17	120.83	415	2	Lee et al., 2010
Yonglong CY	31.78	120.44	5	3	Zhang et al., 2004
Hangzhou HZ3	30.30	120.33	6	4	Liu et al., 2007
Xinhua XH1	32.93	119.83	2	3	Shu et al., 2008
ZK01	31.77	119.80	6	2	Shu et al., 2007
Chifeng	43.97	119.37	503	2	Xu et al., 2002
SZK1	26.08	119.31	9	1	Zheng et al., 2002
Gucheng	31.28	118.90	6	4	Yang et al., 1996
Lulong	39.87	118.87	23	2	Kong et al., 2000
Hulun Lake	48.92	117.42	545	1	Wen et al., 2010
CH-1	31.56	117.39	5	2	Wang et al., 2008
Sanyi profile	43.62	117.38	1598	4	Wang et al., 2005
Xiaoniuchang	42.62	116.82	1411	1	Liu et al., 2002
Haoluku	42.87	116.76	1333	2	Liu et al., 2002
Liuzhouwan	42.71	116.68	1410	7	Liu et al., 2002
Poyang Lake 103B	28.87	116.25	16	4	Jiang and Piperno, 1999
Baiyangdian	38.92	115.84	8	2	Xu et al., 1988
Bayanchagan	42.08	115.35	1355	1	Jiang et al., 2006
Huangjiapu	40.57	115.15	614	7	Sun et al., 2001
Dingnan	24.68	115.00	250	2	Xiao et al., 2007
Guang1	36.02	114.53	56	1	Zhang et al., 2007
Angulinao	41.33	114.35	1315	1	Wang et al., 2010
Yangyuanxipu	40.12	114.22	921	6	Wang et al., 2003

Shenzhen Sx07	22.75	113.78	2	2	Zhang and Yu, 1999
GZ-2	22.71	113.51	1	7	Wang et al., 2010
Daihai99a	40.55	112.66	1221	2	Xiao et al., 2004
Daihai	40.55	112.66	1221	2	Sun et al., 2006
Sihenan profile	34.80	112.40	251	1	Sun and Xia, 2005
Diaojiaohaizi	41.30	112.35	2015	1	Yang et al., 2001
Ganhaizi	39.00	112.30	1854	3	Meng et al., 2007
Jiangling profile	30.35	112.18	37	1	Xie et al., 2006
Helingeer	40.38	111.82	1162	3	Li et al., 2011
Shennongjia2	31.75	110.67	1700	1	Liu et al., 2001
Huguangyan Maar Lake B	21.15	110.28	59	2	Wang et al., 2007
Yaoxian	35.93	110.17	1556	2	Li et al., 2003
Jixian	36.00	110.06	1005	6	Xia et al., 2002
Shennongjia Dajiu Lake	31.49	110.00	1760	2	Zhu et al., 2006
Qigai nuur	39.50	109.85	1300	1	Sun and Feng, 2013
Beizhuangcun	34.35	109.53	519	1	Xue et al., 2010
Lantian	34.15	109.33	523	1	Li and Sun, 2005
Bahanniao	39.32	109.27	1278	1	Guo et al., 2007
Midiwan	37.65	108.62	1400	1	Li et al., 2003
Jinbian	37.50	108.33	1688	2	Cheng, 2011
Xindian	34.38	107.80	608	1	Xue et al., 2010
Nanguanzhuang	34.43	107.75	702	1	Zhao et al., 2003
Xifeng	35.65	107.68	1400	3	Xu, 2006
Jiyuan	37.13	107.40	1765	3	Li et al., 2011
Jiacunyuan	34.27	106.97	1497	2	Gong, 2006
Dadiwan	35.01	105.91	1400	1	Zou et al., 2009
Maying	35.34	104.99	1800	1	Tang and An, 2007
Huiningxiaogou	36.10	104.90	1750	2	Wu et al., 2009
Sujiawan	35.54	104.52	1700	2	Zou et al., 2009
QTH02	39.07	103.61	1302	1	Yu et al., 2009
Laotanfang	26.10	103.20	3579	2	Zhang et al., 2007
Hongshui River2	38.17	102.76	1511	1	Ma et al., 2003,
Ruoergai	33.77	102.55	3480	1	Cai, 2008
Hongyuan	32.78	102.52	3500	2	Wang et al., 2006
Dahaizi	27.50	102.33	3660	1	Li et al., 1988
Shayema Lake	28.58	102.22	2453	1	Tang and Shen, 1996
Luanhaizi	37.59	101.35	3200	5	Herzschuh et al., 2006
Lugu Lake	27.68	100.80	2692	1	Zheng et al., 2014
Qinghai Lake	36.93	100.73	3200	2	Shen et al., 2004
Dalianhai	36.25	100.41	2850	3	Cheng et al., 2010
Erhai ES Core	25.78	100.19	1974	1	Shen et al., 2006
Xianmachi profile	25.97	99.87	3820	7	Yang et al., 2004

TCK1	26.63	99.72	3898	1	Xiao et al., 2014
Yidun Lake	30.30	99.55	4470	4	Shen et al., 2006
Kuhai lake	35.30	99.20	4150	1	Wischnewski et al., 2011
Koucha lake	34.00	97.20	4540	2	Herzschuh et al., 2009
Hurleg	37.28	96.90	2817	2	Zhao et al., 2007
Basu	30.72	96.67	4450	3	Tang et al., 1998
Tuolekule	43.34	94.21	1890	1	An et al., 2011
Balikun	43.62	92.77	1575	1	Tao et al., 2010
Cuona	31.47	91.51	4515	3	Tang et al., 2009
Dongdaohaizi2	44.64	87.58	402	1	Li et al., 2001
Bositeng Lake	41.96	87.21	1050	1	Xu, 1998
Cuoqin	31.00	85.00	4648	4	Luo, 2008
Yili	43.86	81.97	928	2	Li et al., 2011
Bangong Lake	33.75	78.67	4241	1	Huang et al., 1996
Shengli	47.53	133.87	52	2	CQPD, 2000
Qingdeli	48.05	133.17	52	1	CQPD, 2000
Changbaishan	42.22	126.00	500	2	CQPD, 2000
Liuhe	42.90	125.75	910	7	CQPD, 2000
Shuangyang	43.27	125.75	215	1	CQPD, 2000
Xiaonan	43.33	125.33	209	1	CQPD, 2000
Tailai	46.40	123.43	146	5	CQPD, 2000
Sheli	45.23	123.31	150	4	CQPD, 2000
Tongtu	45.23	123.30	150	7	CQPD, 2000
Yueyawan	37.98	120.71	5	1	CQPD, 2000
Beiwangxu	37.75	120.61	6	1	CQPD, 2000
East Tai Lake1	31.30	120.60	3	1	CQPD, 2000
Suzhou	31.30	120.60	2	7	CQPD, 2000
Sun-Moon Lake	23.51	120.54	726	2	CQPD, 2000
West Tai Lake	31.30	119.80	1	1	CQPD, 2000
Changzhou	31.43	119.41	5	1	CQPD, 2000
Dazeyin	39.50	119.17	50	7	CQPD, 2000
Hailaer	49.17	119.00	760	2	CQPD, 2000
Cangumiao	39.97	118.60	70	1	CQPD, 2000
Qianhuzhuang	40.00	118.58	80	6	CQPD, 2000
Reshuitang	43.75	117.65	1200	1	CQPD, 2000
Yangerzhuang	38.20	117.30	5	7	CQPD, 2000
Mengcun	38.00	117.06	7	5	CQPD, 2000
Hanjiang-CH2	23.48	116.80	5	2	CQPD, 2000
Hanjiang-SH6	23.42	116.68	3	7	CQPD, 2000
Hanjiang-SH5	23.45	116.67	8	2	CQPD, 2000
Hulun Lake	48.90	116.50	650	1	CQPD, 2000
Heitutang	40.38	113.74	1060	1	CQPD, 2000
Zhujiang delta PK16	22.73	113.72	15	7	CQPD, 2000

Angulitun	41.30	113.70	1400	7	CQPD, 2000
Bataigou	40.92	113.63	1357	1	CQPD, 2000
Dahewan	40.87	113.57	1298	2	CQPD, 2000
Yutubao	40.75	112.67	1254	7	CQPD, 2000
Zhujiang delta K5	22.78	112.63	12	1	CQPD, 2000
Da-7	40.52	112.62	1200	3	CQPD, 2000
Hahai-1	40.17	112.50	1200	5	CQPD, 2000
Wajianggou	40.50	112.50	1476	4	CQPD, 2000
Shuidong Core A1	21.75	111.07	-8	2	CQPD, 2000
Dajahu	31.50	110.33	1700	2	CQPD, 2000
Tianshuigou	34.87	109.73	360	7	CQPD, 2000
Mengjiawan	38.60	109.67	1190	7	CQPD, 2000
Fuping BK13	34.70	109.25	422	7	CQPD, 2000
Yaocun	34.70	109.22	405	2	CQPD, 2000
Jinbian	37.80	108.60	1400	4	CQPD, 2000
Dishaogou	37.83	108.45	1200	2	CQPD, 2000
Shuidonggou	38.20	106.57	1200	5	CQPD, 2000
Jiuzhoutai	35.90	104.80	2136	7	CQPD, 2000
Luojishan	27.50	102.40	3800	1	CQPD, 2000
RM-F	33.08	102.35	3400	2	CQPD, 2000
Hongyuan	33.25	101.57	3492	1	CQPD, 2000
Wasong	33.20	101.52	3490	1	CQPD, 2000
Guhu Core 28	27.67	100.83	2780	7	CQPD, 2000
Napahai Core 34	27.80	99.60	3260	2	CQPD, 2000
Lop Nur	40.50	90.25	780	7	CQPD, 2000
Chaiwobao1	43.55	87.78	1100	2	CQPD, 2000
Chaiwobao2	43.33	87.47	1114	1	CQPD, 2000
Manasi	45.97	84.83	257	2	CQPD, 2000
Wuqia	43.20	83.50	1000	7	CQPD, 2000
Madagou	37.00	80.70	1370	2	CQPD, 2000
Tongyu	44.83	123.10	148	5	CQPD, 2000
Nanjing	32.15	119.05	10	2	CQPD, 2000
Banpo	34.27	109.03	395	1	CQPD, 2000
QL-1	34.00	107.58	2200	7	CQPD, 2000
Dalainu	43.20	116.60	1290	7	CQPD, 2000
Qinghai	36.55	99.60	3196	2	CQPD, 2000

Table 2. Earth's orbital parameters and trace gases as recommended by the PMIP3 project

Simulation	Orbital parameters			Trace gases		
	Eccentricity	Obliquity(°)	Angular precession(°)	CO_2(ppmv)	CH_4(ppbv)	N_2O(ppbv)
PI	0,0167724	23,446	102,04	280	760	270
MH	0,018682	24,105	0,87	280	650	270

Table 3. PMIP3 model characteristics and references

Model Name	*Modelling centre*	*Type*	*Grid*	*Reference*
BCC-CSM-1-1	BCC-CMA (China)	AOVGCM	Atm: 128×64×L26; Ocean: 360×232×L40	Xin et al. (2013)
CCSM4	NCAR (USA)	AOGCM	Atm: 288 × 192×L26; Ocean: 320×384×L60	Gent et al. (2011)
CNRM-CM5	CNRM&CERFACS (France)	AOGCM	Atm: 256 × 128×L31; Ocean: 362×292×L42	Voldoire et al. (2012)
CSIRO-Mk3-6-0	QCCCE, Australia	AOGCM	Atm: 192 × 96×L18; Ocean: 192×192×L31	Jeffrey et al. (2013)
FGOALS-g2	LASG-IAP (China)	AOVGCM	Atm: 128 × 60×L26; Ocean: 360×180×L30	Li et al. (2013)
FGOALS-s2	LASG-IAP (China)	AOVGCM	Atm: 128 × 108×L26; Ocean: 360×180×L30	Bao et al. (2013)
GISS-E2-R	GISS (USA)	AOGCM	Atm: 144 × 90×L40; Ocean: 288×180×L32	Schmidt et al. (2014a,b)
HadGEM2-CC	Hadley Centre (UK)	AOVGCM	Atm: 192 × 145×L60; Ocean: 360×216×L40	Collins et al. (2011)
HadGEM2-ES	Hadley Centre (UK)	AOVGCM	Atm: 192 × 145×L38; Ocean: 360×216×L40	Collins et al. (2011)
IPSL-CM5A-LR	IPSL (France)	AOVGCM	Atm: 96 × 96×L39; Ocean: 182×149×L31	Dufresne et al. (2013)
MIROC-ESM	Utokyo&NIES (Japan)	AOVGCM	Atm: 128×64×L80; Ocean: 256×192×L44	Watanabe et al. (2011)
MPI-ESM-P	MPI (Germany)	AOGCM	Atm: 196×98×L47; Ocean: 256×220×L40	Giorgetta et al. (2013)
MRI-CGCM3	MRI (Japan)	AOGCM	Atm: 320 × 160×L48; Ocean: 364×368×L51	Yukimoto et al. (2012)

Table 4. Important values for each plant life form used in the ΔV statistical calculation as assigned to the megabiomes

Megabiomes	*Life form*		
	Trees	**Grass/grass**	**Bare ground**
Tropical forest	1		
Warm mixed forest	1		
Temperate forest	1		
Boreal forest	1		
Grassland and dry shrubland	0.25	0.75	
Savanna and dry woodland	0.5	0.5	
Desert		0.25	0.75
Tundra		0.75	0.25

Table 5. Attribute values and the weights for plant life forms used by the ΔV statistic

Life form	*Attribute*			
Trees	Evergreen	Needle-leaf	Tropical	Boreal
Tropical forest	1	0	1	0
Warm mixed forest	0.75	0.25	0	0
Temperate forest	0.5	0.5	0	0.5
Boreal forest	0.25	0.75	0	1
Grassland and dry shrubland	0.75	0.25	0.75	0
Savanna and dry woodland	0.25	0.75	0	0.5
weights	0.2	0.2	0.3	0.3
Grass/Shrub	Warm	Arctic/alpine		
Grassland and dry shrubland	1	0		
Savanna and dry woodland	0.75	0		
Desert	1	0		
Tundra	0	1		
weights	0.5	0.5		
Bare Ground	Arctic/alpine			
Desert	0			
Tundra	1			
weight	1			

Table 6. Regression coefficients between the reconstructed climates by inverse vegetation models and observed meteorogical values

Climate parameter	Slope	Intercept	R	ME	RMSE
MAT	0..82±0..02	0.92±0.18	0.89	0.16	3.25
MTCO	0.81±0.01	-1.79±0.18	0.95	-0.17	3.19
MTWA	0.75±0.03	4.57±0.60	0.75	-0.19	4.02
MAP	1.15±0.02	32.90±18.41	0.94	138.01	263.88
Pjan	1.01±0.02	0.32±0.47	0.94	0.52	8.89
Pjul	1.30±0.03	-21.67±4.52	0.89	16.45	52.9

The climatic parameters used for regression are the actual values (data source: China Climate Bureau, China Ground Meteorological Record Monthly Report, 1951-2001). MAT annual mean temperature, MTCO mean temperature of the coldest month, MTWA mean temperature of the warmest month, MAP annual precipitation, RMSE the root-mean-square error of the residuals, ME mean error of the residuals, Pjan: precipitation of January, Pjul: precipitation of July, R is the correlation coefficient, ± stand error

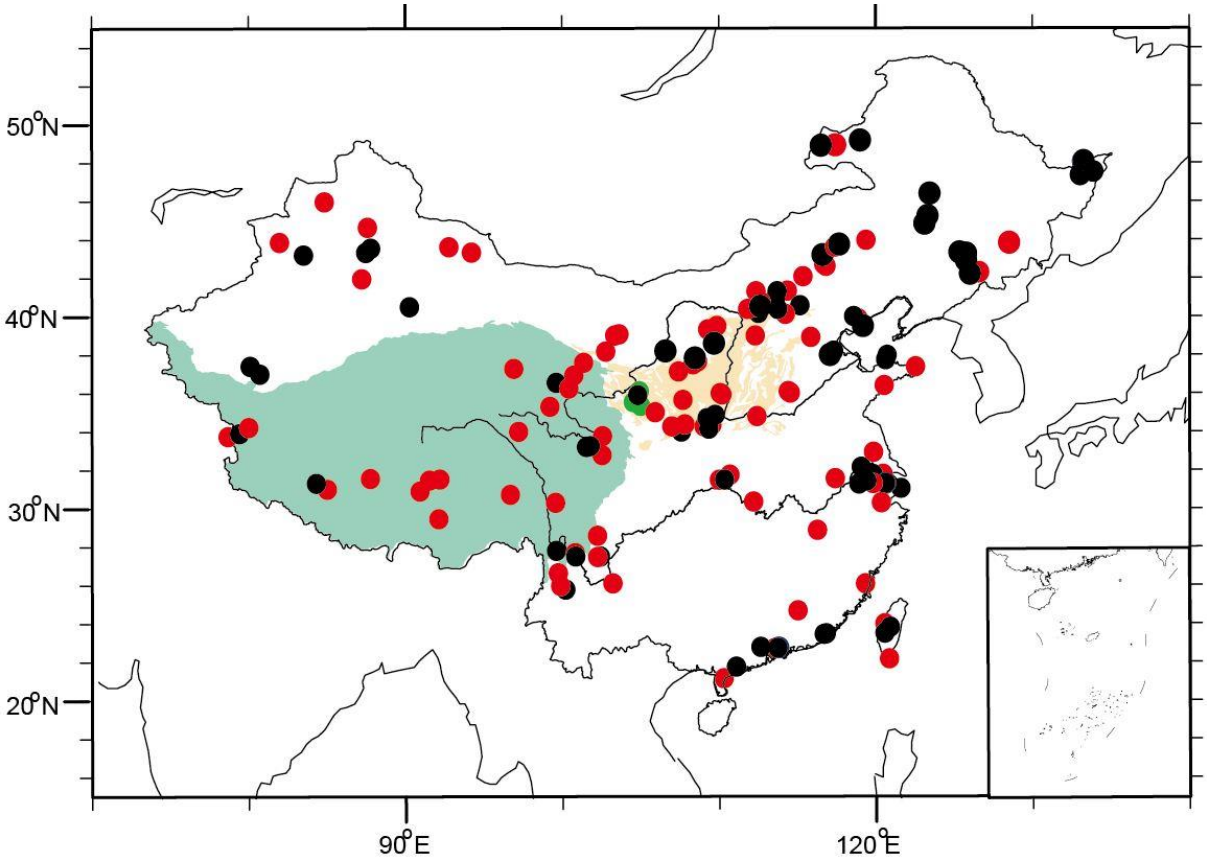

Figure 1. Distribution of pollen sites during mid-Holocene period in China. Black circle is the original China Quaternary Pollen Database, red circles are digitized ones from published papers, green circles represent the three original pollen data used in this study. The area with green color represents the Tibetan Plateau, yellow color for the Loess Plateau.

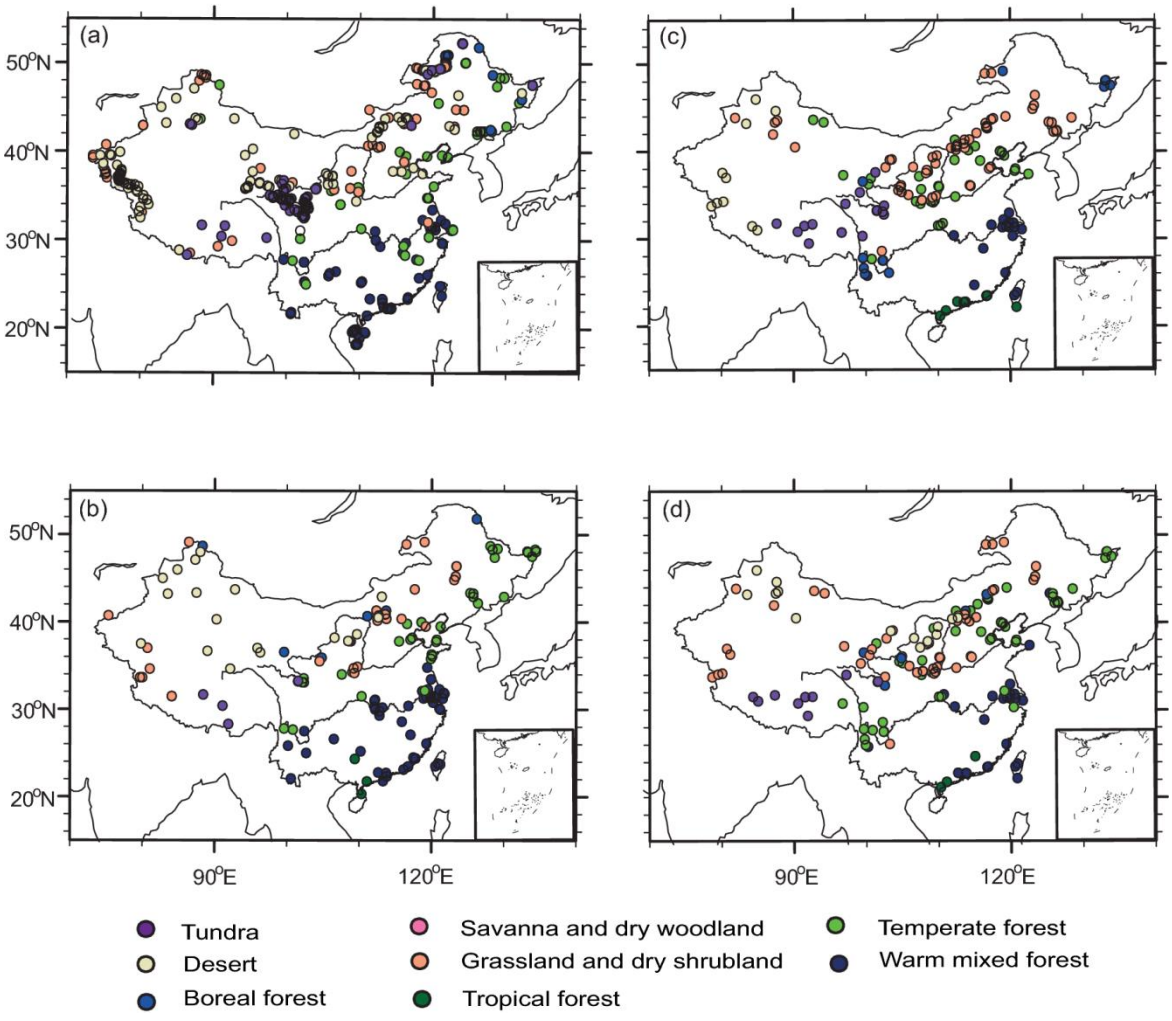

Figure 2. Comparison of megabiomes for PI (first row) and the MH (second row): (a,b) BIOME6000, (c,d) pollen data collected in this study.

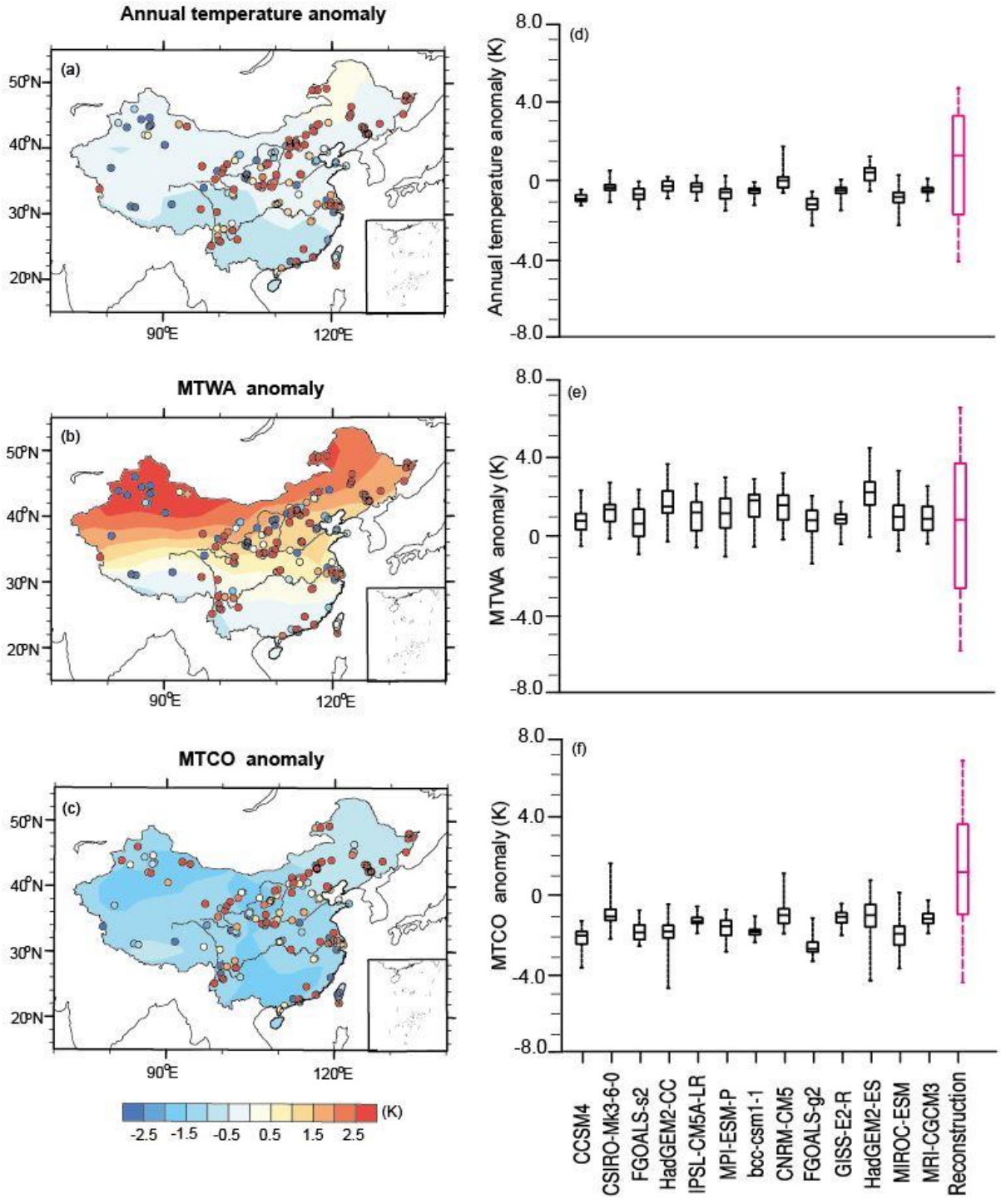

Figure 3. Model-data comparison for annual and seasonal (MTWA and MTCO) temperature (K). For the left panel (a-c), points represent the reconstruction from IVM, shades show the last 30-year means simulation results of multi-model ensemble (MME) for 13 PMIP3 models. The box-and-whisker plots (d-f) show the changes as shown by each PMIP3 model and the reconstruction. (d) considers changes in annual temperature, (e) indicates changes in MTWA, and (f) shows changes in MTCO. The lines in each box shows the median value from each set of measurements, the box shows the 25%-75% range, and the whiskers show the 90% interval (5th to 95th percentile).

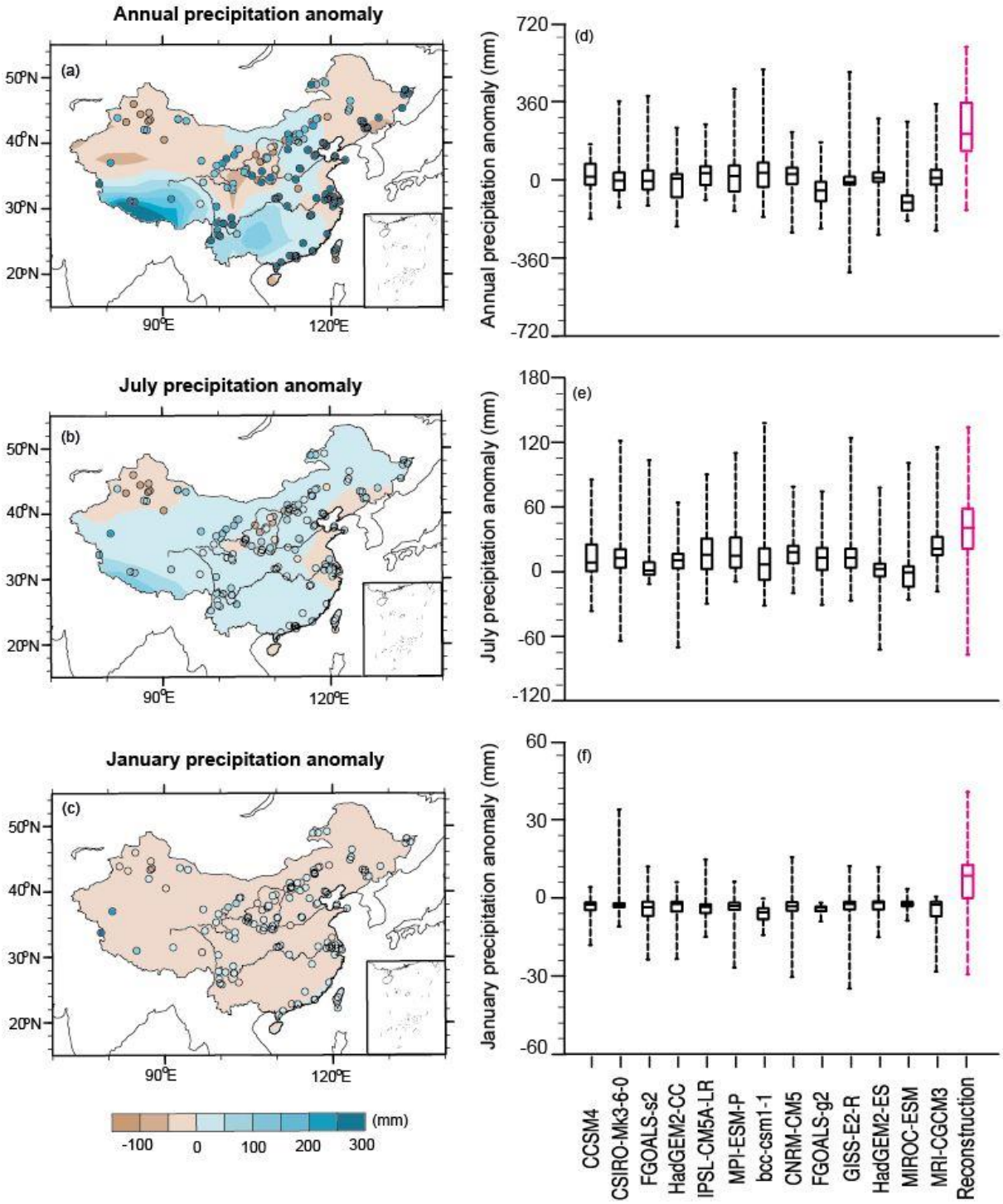

Figure 4. Model-data comparison for annual, July and January precipitation (mm). For the left panel (a,b), points represent the reconstruction from IVM, shades show the last 30-year means simulation results of multi-model ensemble (MME) for 13 PMIP3 models. The box-and-whisker plots (d-f) show the changes as shown by each PMIP3 model and the reconstruction. (d) considers changes in annual precipitation, (e) indicates changes in July precipitation, and (f) shows changes in January precipitation. The lines in each box shows the median value from each set of measurements, the box shows the 25%-75% range, and the whiskers show the 90% interval (5th to 95th percentile).

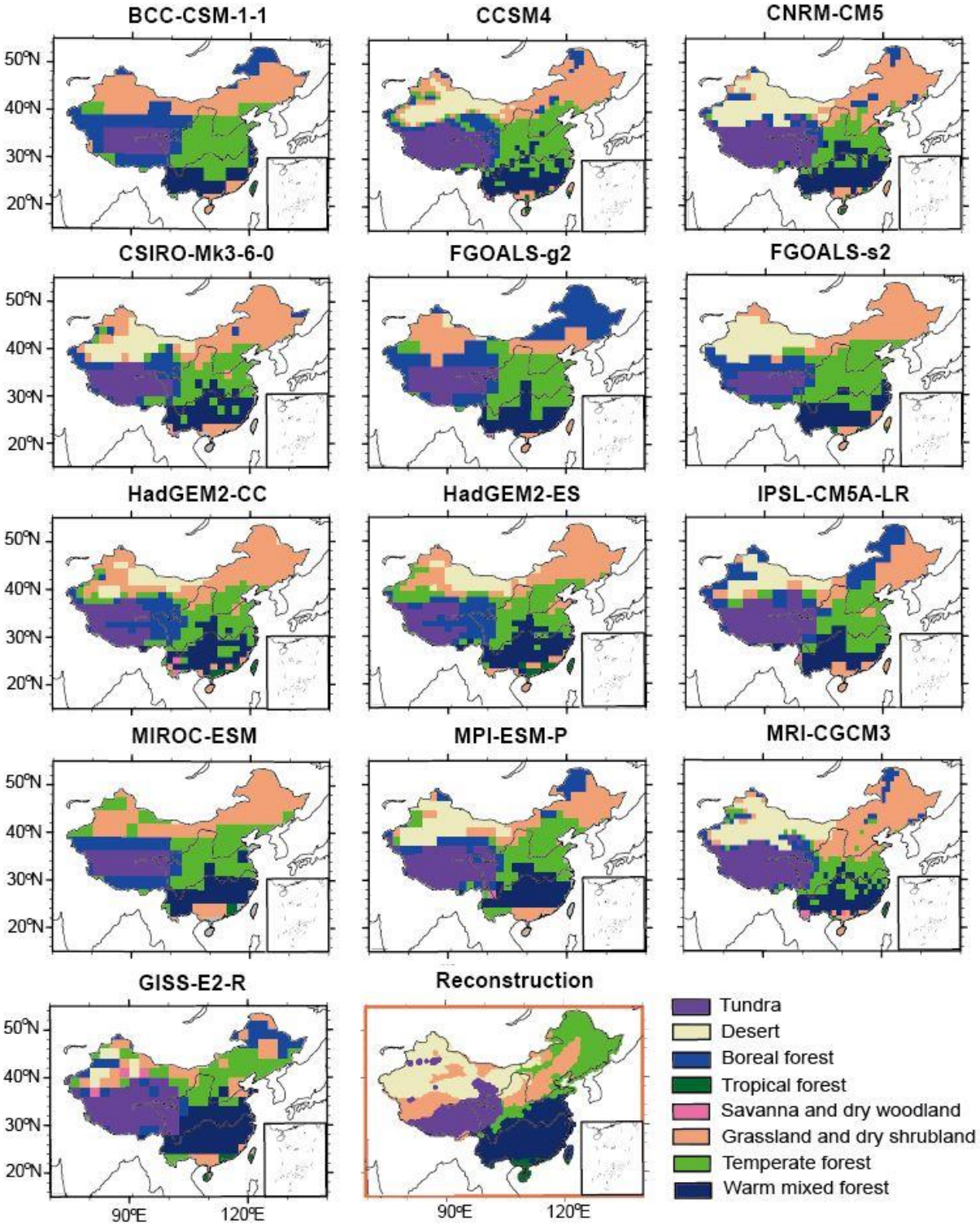

Figure 5. Comparison of interpolated megabiomes distribution (plot in red rectangle) with the simulated spatial pattern from BIOME4 for each model during mid-Holocene.

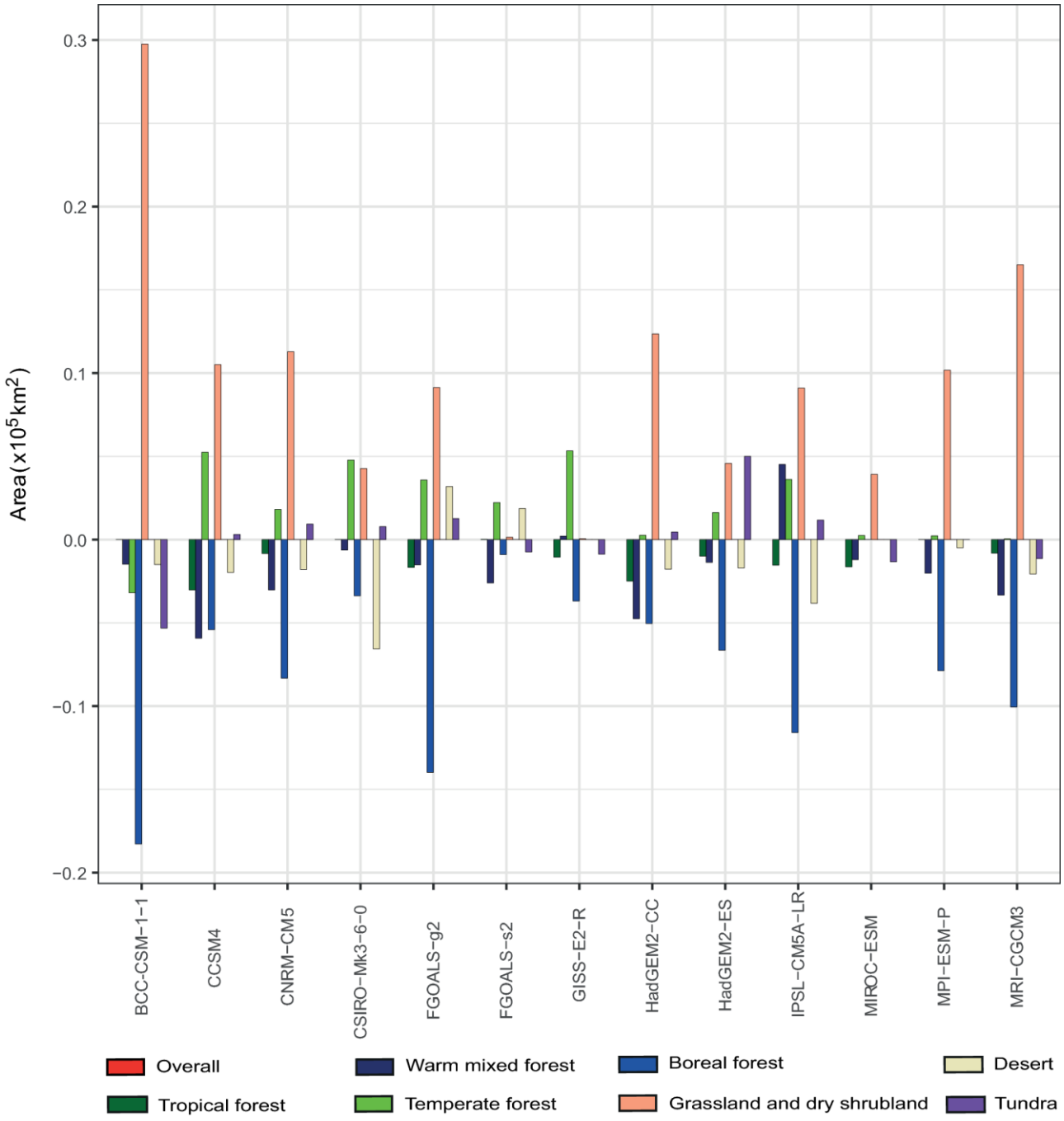

Figure 6. Changes in the extent of each megabiome as a consequence of simulated climate changes for each model, both expressed as change relative to the PI extent of same megabiome.

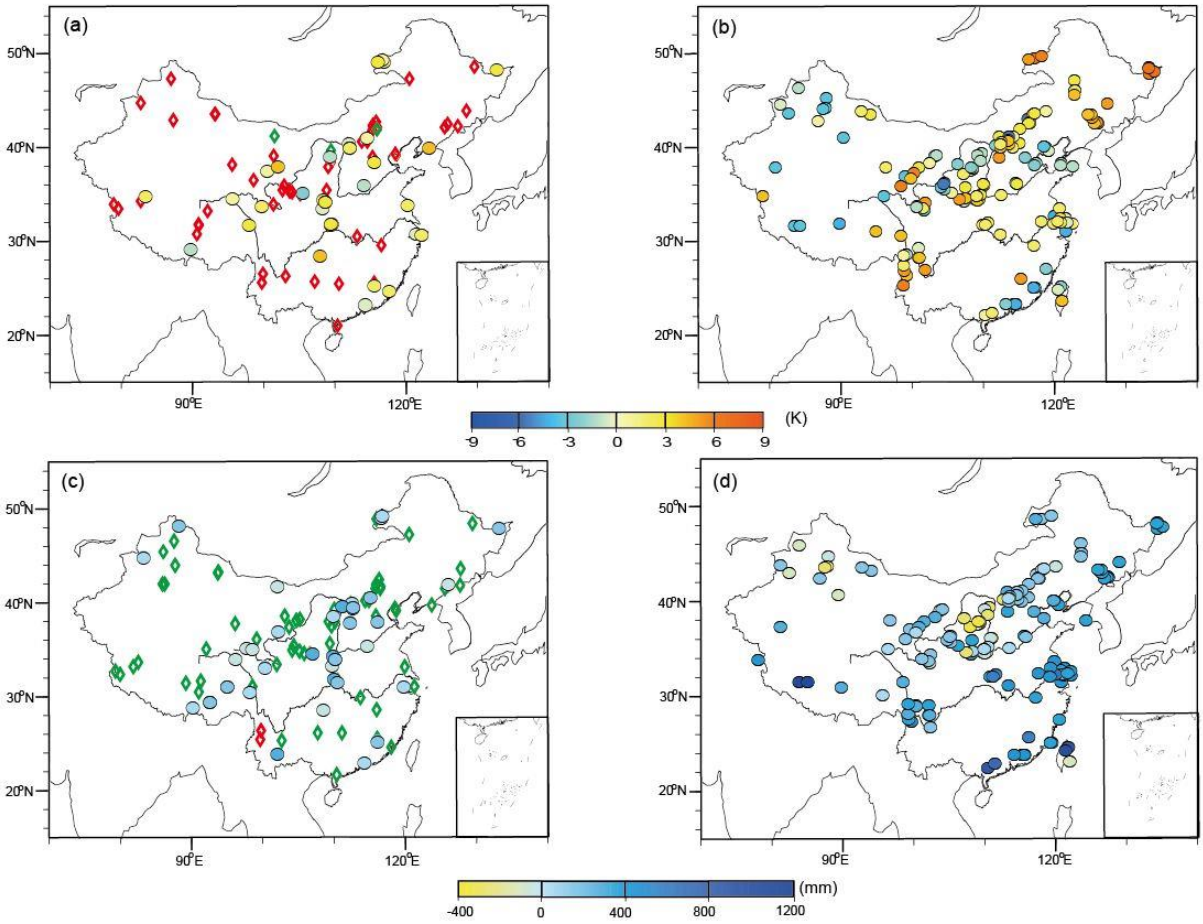

Figure 7. Comparison between the climate reconstruction and previous reconstruction over China. (a) Previous temperature results. Diamond is the qualitative reconstruction, red is the temperature increase and green is the temperature decrease; Circle is quantitative reconstruction; (b) Mean annual temperature reconstruction in this study; (c) Previous precipitation results, diamond is the qualitative reconstruction, red is the precipitation decrease and green is the precipitation increase; Circle is the quantitative reconstruction; (d) Mean annual precipitation reconstruction in this study.

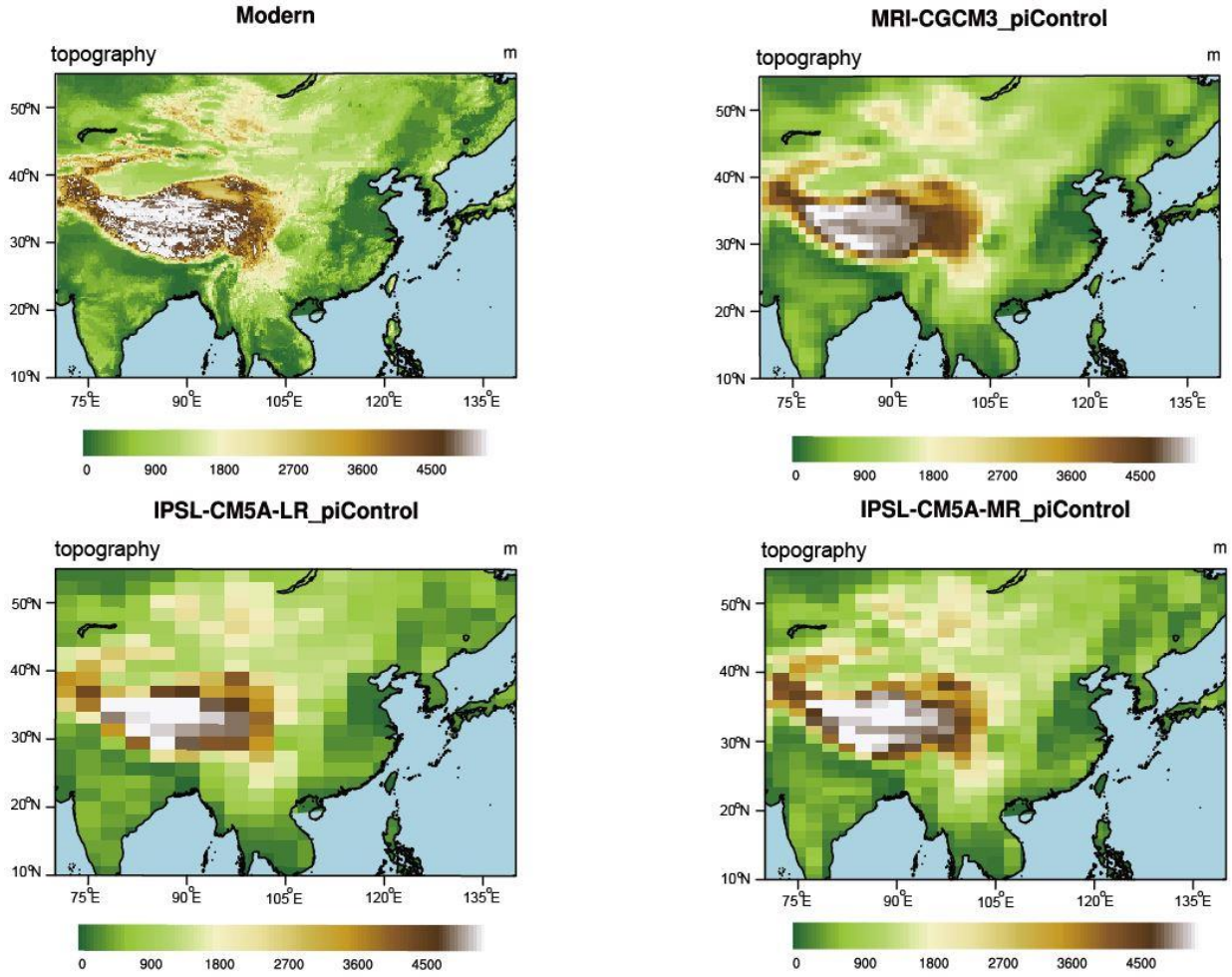

Figure 8. The topography comparison between models and observation.

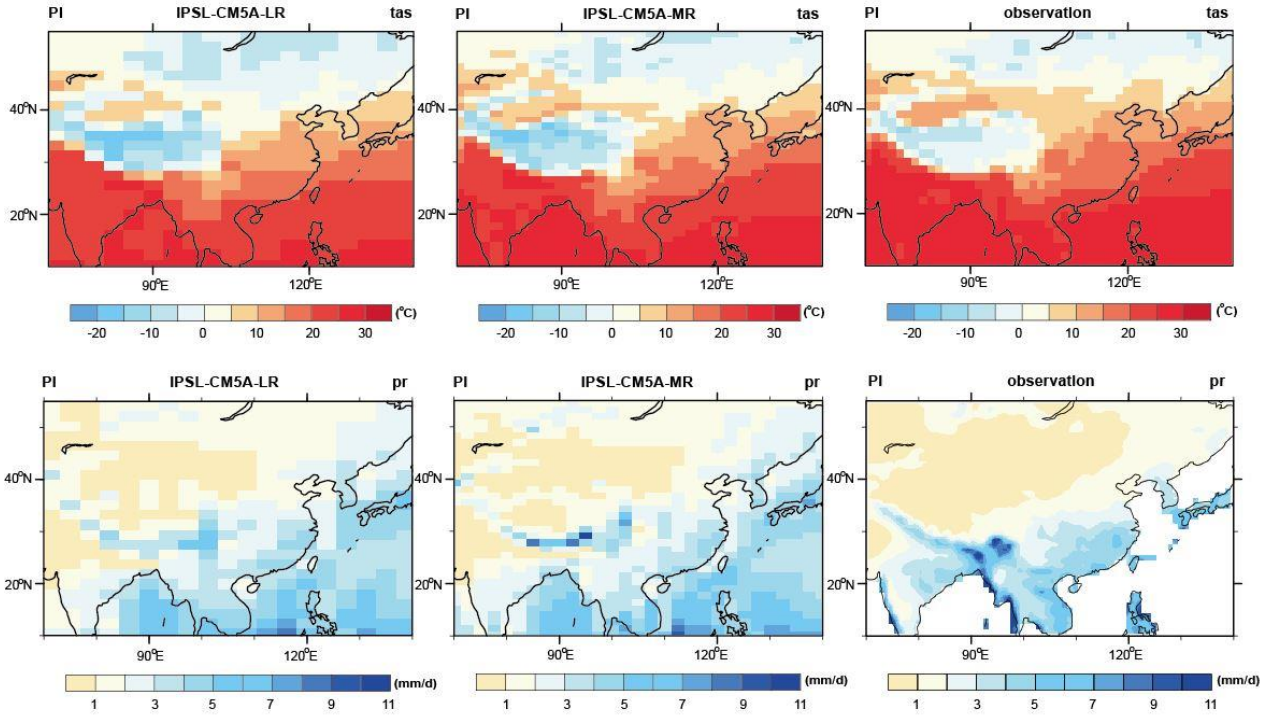

Figure 9. The preindustrial climate comparison between simulation and observation. Tas means temperature above 2m surface, pr means precipitation.

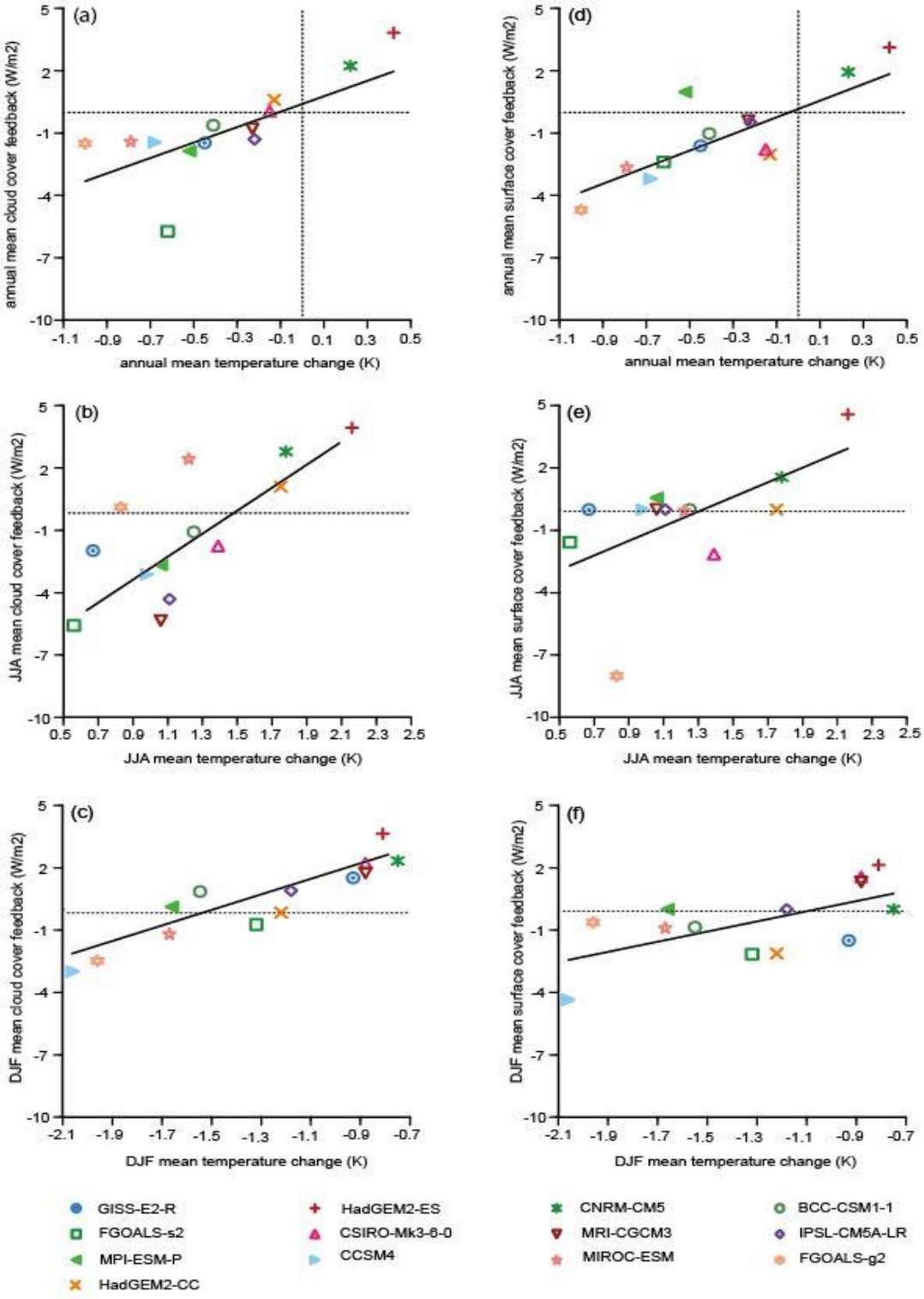

Figure 10. Scatter plots showing temperature, cloud cover feedback and surface albedo feedback changes during the MH. The values shown are the simulated 30-year mean anomaly (MH-PI) for the 13 models. **a**, annual mean temperature relative to the annual mean cloud cover feedback and d, annual surface albedo feedback. b, Summer (JJA) mean temperature relative to the summer mean cloud cover feedback and **e**, Summer surface albedo feedback. **c**, Winter (DJF) mean temperature relative to the summer mean cloud cover feedback and **f**, Winter surface albedo feedback. The horizontal and vertical lines in plots represent the value of 0.

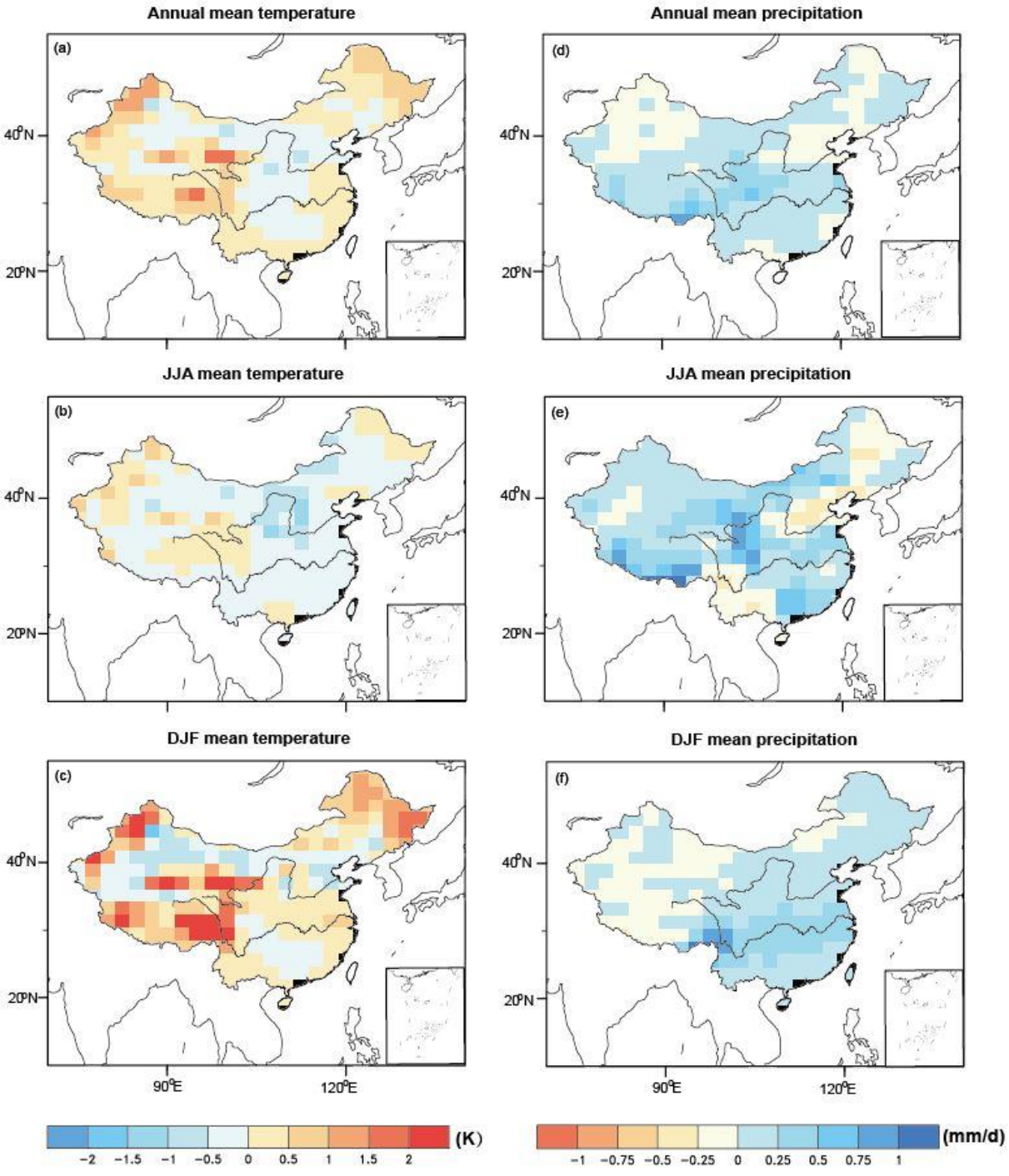

Figure 11. Climate anomalies between the two experiments (6 ka and 6 ka_VEG) conducted in CESM version 1.0.5. The anomalies (6 ka_VEG-6 ka) of temperature and precipitation at both annual and seasonal scale are presented, and all these climate variables are calculated as the last 50-year means from two simulations.